16 Dynamics of fluid flow in Martian outflow channels

LIONEL WILSON,
ALISTAIR S. BARGERY
and DEVON M. BURR

Summary

The conditions under which large volumes of water may have flowed at high speeds across the surface of Mars are considered. To assess the likely ranges of initial water temperature and release rate, the possible conditions in subsurface aquifers confined beneath the cryosphere are explored. Then the transfer of water to the surface in fractures induced by volcanic activity or tectonic events is modelled and the physical processes involved in its release into the Martian environment are discussed. The motion of the water across the surface is analysed with standard treatments for fluvial systems on Earth, modified for Mars by taking account of the differing environmental conditions and removing what may be considered to be the unsafe assumption that most channels involved bankfull flows. The most commonly discussed environmental difference is the smaller acceleration due to gravity on Mars. However, an important additional factor may have been the initially vigorous evaporation of water into the low-pressure Martian atmosphere. This process, together with the thermal losses incurred by assimilation of very cold rock and ice eroded from the cryosphere over which the water travels, causes minor changes in the depth and speed of a water flood but, eventually, produces major changes in the flood rheology as the total ice and sediment loads increase. The roles of these processes in determining the maximum distance to which the water may travel, and the relative importance of erosion and deposition in its bed, are discussed.

16.1 Introduction

Since the recognition of the Martian outflow channels in the imaging data from the Viking missions (Sharp and Malin, 1975; Masursky *et al.*, 1977; Komar, 1980; Carr and Clow, 1981), and the realisation that, despite alternative suggestions (Milton, 1974; Hoffman, 2000, 2001; Leverington, 2004), flowing water was the most likely mechanism for their formation (Baker, 1979; Carr, 1979; Komar, 1979; Baker, 2001; Coleman, 2003), it has been appreciated that the great size of the channels probably implies extreme flow conditions. Depending on the assumptions made about the depths of water in the channels and the relevant flow regimes, various authors have obtained estimates of the peak discharges that mainly range between $\sim 10^6$ and $10^8\,m^3\,s^{-1}$ (Carr, 1979; Komar, 1979; De Hon and Pani, 1993; Komatsu and Baker, 1997; Ori and Mosangini, 1998; Williams *et al.*, 2000; Burr *et al.*, 2002a, b; Chapman *et al.*, 2003; Head *et al.*, 2003a; Coleman, 2004; Leask *et al.*, 2006a, 2007) but extend up to $10^{10}\,m^3\,s^{-1}$ (Robinson and Tanaka, 1990; Dohm *et al.*, 2001a, 2001b). Table 16.1 summarises a representative range of examples. Here, the key factors involved in determining water flow conditions in outflow channels, including the limitations imposed by the likely nature of the subsurface water sources and the mechanisms of water release to the surface, are reviewed. The consequences for water flow on the Martian surface, under environmental conditions of low temperature, low atmospheric pressure, and low acceleration due to gravity are explored. Suggestions are made as to how some of the assumptions made in previous work may be improved, significantly reducing the largest implied discharges, and giving explicit estimates of discharge and flow conditions in several named channels.

16.2 Water sources

The morphologies of the source regions of most Martian outflow channels, including areas of chaos (Coleman and Baker, this volume Chapter 9) and graben (Burr *et al.*, this volume Chapter 10), suggest that the water forming the channels was released from a significant depth beneath the surface. In a few cases, release of water from ice-covered lakes has been suggested (Komatsu *et al.*, 2004; Woodworth-Lynas and Guigné, 2004). Elsewhere, a small number of deeply incised valley networks originate at large basins, implying flooding due to basin overflow as a result of runoff and/or groundwater inflow (Irwin and Grant, this volume Chapter 11). The largest flood channels on Mars, however, originate from chaotic terrain and graben.

Although graben systems can be formed by purely tectonic forces (Hanna and Phillips, 2006), an origin involving the additional stress change due to dyke intrusion has been proposed for many of them (Rubin, 1992; Chadwick and Embly, 1998; Wilson and Head, 2002, 2004; Leask *et al.*, 2006b), and an origin due to sill intrusion is a natural explanation for at least some areas of chaos (Scott and Wilson, 1999; Ogawa *et al.*, 2003; Nimmo and Tanaka, 2005; Leask *et al.*, 2006c), though geothermal melting of a

Megaflooding on Earth and Mars, ed. Devon M. Burr, Paul A. Carling and Victor R. Baker.
Published by Cambridge University Press.

Table 16.1. Outflow channel parameters

Valley	Source	Estimated flux ($m^3\ s^{-1}$)	Fracture length (km)	Implied aquifer permeability (m^2)
(W. Tharsis)[a]	(Hidden)	10^9-10^{10}	1000?	8.0×10^{-6}?
Kasei[b]	Echus Chasma	$9–23 \times 10^8$	130–500?	$>1.4 \times 10^{-5}$?
Ares[c]	Ianni Chaos	10^8-10^9	360	2.2×10^{-6}
Hydraotes[d]	Hydraotes Chaos	$7–40 \times 10^7$	500?	1.1×10^{-6}
Tiu[d]	Hydraotes Chaos	$3–20 \times 10^7$	500?	4.8×10^{-7}?
Maja[e]	Juventae Chasma	9×10^7	240?	3.0×10^{-6}?
Mangala[f]	Memnonia Fossa	$1–8 \times 10^7$	223	4.0×10^{-7}
Simud[d]	Hydraotes Chaos	$1–5 \times 10^7$	500?	1.6×10^{-7}?
Mangala[g]	Memnonia Fossa	$8–40 \times 10^6$	210	3.2×10^{-7}
Ravi[h]	Aromatum Chaos	$3–30 \times 10^6$	50	4.8×10^{-7}
Athabasca[i]	Cerberus Fossae	$2–4 \times 10^6$	35	4.4×10^{-7}

[a] Dohm *et al.* (2001a, 2001b), [b] Robinson and Tanaka (1990), [c] Komatsu and Baker (1997), [d] Ori and Mosangini (1998), [e] De Hon and Pani (1993), [f] Ghatan *et al.* (2005), [g] Komar (1979), [h] Leask *et al.* (2004), [i] Burr *et al.* (2002a, 2002b); Head *et al.* (2003a).

buried crater-floor lake has been proposed for Aram Chaos (Oost-hoek *et al.*, 2007). At first sight it is tempting to suggest that the released water could consist entirely of ice melted by the heat from the intrusion (McKenzie and Nimmo, 1999). However, in the two cases that have been examined in detail, the Mangala Fossa graben source of the Mangala Valles channel system (Leask *et al.*, 2006b) and the Aromatum Chaos source of Ravi Vallis (Leask *et al.*, 2006c), it has been shown that the volume of water that could be melted by the relevant volcanic intrusion was too small by at least two orders of magnitude to explain the transport of the volume of crustal material eroded to form the channel. Thus it appears that, in most cases where a volcanic event was involved, its main physical role was to fracture the crust and release pre-existing liquid water trapped beneath the surface (though there may be other, chemical and thermal, consequences discussed in the next section).

An abundance of confined aquifers is to be expected on Mars as a consequence of the likely presence, for much of the history of the planet, of a cryosphere, in which any water is present as ice in pore spaces and fractures in the shallow crustal rocks (Rossbacher and Judson, 1981; Clifford, 1987, 1993; Clifford and Parker, 2001; Carr, 2002). Given plausible values for the geothermal heat flux at various times in Martian history of 20–30 $mW\ m^{-2}$ (McGovern *et al.*, 2002) and for the thermal conductivity of the cryosphere ($\sim$2.5 $W\ m^{-1}\ K^{-1}$ – Leask *et al.*, 2006c), the requirements that the temperature be close to the modern average value ($\sim$210 K) at the surface and $\sim$273 K at the top of the aquifer lead to estimates of the depths, D, to the tops of aquifers in the range 5 to 8 km, somewhat larger than the $\sim$2.3 to 6.5 km range in the preferred model of Clifford (1993). However, significantly shallower aquifers are possible locally in areas of abnormally high heat flow (Gulick, 1998, 2001; Coleman, 2005) or reduced thermal conductivity (Mellon and Phillips, 2001; Heldmann and Mellon, 2004; Edlund and Heldmann, 2006) and $D = 3.5$ km is used in calculations below. The levels of stress generated by tectonic events (Hanna and Phillips, 2006) and volcanic dyke and sill intrusions (Wilson and Head, 2004) on Mars appear to be quite adequate to fracture a several-kilometre thickness of cryosphere to provide pathways for water release.

16.3 Water ascent to the surface

To obtain realistic inputs to models of water flow on the surface of Mars the ascent of water to the surface from deep aquifer systems needs consideration. The speed at which water can flow up an open fracture is a function of the excess pressure at the base of the fracture and the fracture width. However, these variables are also linked to the conditions in the underlying aquifer and the stress field that induces the fracture. Modelling calculations using coupled models of fracture formation and aquifer properties have been made for the Cerberus Fossae source graben of the Athabasca Valles by Manga (2004) and Hanna and Phillips (2006), and for the Mangala Fossa source graben of the Mangala Valles channel system by Hanna and Phillips (2006). Initial water discharge rates are found to range between $\sim 10^5$ and somewhat in excess of $10^6\ m^3\ s^{-1}$. Discharge is predicted to decay exponentially, on a time scale generally found to be of order hours, as a result of the flow limitations imposed by the permeabilities and compressibilities of the aquifers (Manga, 2004).

Although these discharges are consistent with the smallest values inferred from channel geometries (Table 16.1), they are orders of magnitude smaller than the largest

estimates. This discrepancy can be resolved partly by noting that many of the discharge values in Table 16.1 probably are overestimated greatly, as will be shown below in the section 'Dynamics of water flow'. However, the very great extent of the discrepancy, and especially the inference (see below) that for the larger channels the high discharge rates were maintained for many weeks, not the hours suggested by the existing models, implies that the permeabilities generally inferred for the Martian subsurface in these models, at most $\sim 10^{-11}$ m^2 and decreasing to $\sim 10^{-15}$ m^2 at great depth (Manga, 2004; Hanna and Phillips, 2005), may be much too small. Martian aquifers may extend from the ~4 km depth of the base of the cryosphere down to the ~10 km depth where porosity becomes negligible, making their vertical extents $H \approx 6$ km. The horizontal extents of the fractures delineating some named outflow channel source areas are listed in Table 16.1, and equating the estimated fluxes listed to the product of the aquifer cross-sectional area and the Darcy velocity allows values to be calculated for the aquifer permeabilities that would be required to allow these discharges to take place (Wilson *et al.*, 2004). These values, given in the final column of Table 16.1, are at least $\sim 10^{-7}$ m^2 and are more similar to those commonly associated with loose gravel than to normal aquifers on Earth, though aquifers formed within the rubble tops and bottoms of layers of basaltic lava flows can have significantly greater permeabilities (Saar and Manga, 1999, 2004). If the typical permeability of the Martian crust is indeed much greater than that of the Earth, a possible explanation is that the crustal fractures defining the megaregolith, generated by the early impact bombardment of the planet, have been preserved over geological time. Unfortunately there is no information on the detailed structure of this or any other megaregolith, which on the Moon was detected only indirectly by the Apollo seismic network (Lognonne, 2005) via the scattering of seismic signals. However, it seems reasonable to assume that the Martian megaregolith may contain a network of relatively wide, interconnected fractures with both high porosity and high permeability. If so, an approach using the Darcy law may be inappropriate for modelling water flow through such a structure. Whatever the source of the high permeability, an additional implication would be that there has been no systematic infilling of the fracture systems by secondary minerals (Hanna and Phillips, 2005).

An important parameter determining the fate of water reaching the surface of Mars is its temperature on release, determined by its temperature within the aquifer and the amount of heat lost in transit. The water temperature depends strongly on whether convection is taking place in the aquifer. If it is assumed that no convection takes place, then with a geothermal heat flow of 20 mW m^{-2} and a bulk aquifer thermal conductivity of ~ 1 W m^{-1} K^{-1} the temperature gradient will be 20 K km^{-1}. Over a 6 km vertical extent of aquifer the temperature increase will be 120 K, and because the top of the aquifer is at 0 °C the mean water temperature will be around 60 °C. The criterion for convection to occur (see Section 9–9 in Turcotte and Schubert, 2002) is that the aquifer permeability k must exceed a critical value k_c given by

$$k_c = (4\pi^2 \mu_w K)/(\alpha_w g \rho_w^2 c_w H^2 \, dT/dz), \quad (16.1)$$

where μ_w, α_w, ρ_w and c_w are the viscosity, volume thermal expansion coefficient, density and specific heat at constant pressure, respectively, of the water, K is the bulk thermal conductivity of the aquifer, g is the acceleration due to gravity (3.72 m s^{-2}), H is the aquifer thickness and dT/dz is the temperature gradient across the aquifer. Inserting appropriate values for water at 60 °C in an aquifer 6 km thick, ($\mu_w = 5 \times 10^{-4}$ Pa s, $\alpha_w = 5 \times 10^{-4}$, $\rho_w = 1000$ kg m^{-3}, $c_w = 4175$ J kg^{-1} K^{-1} and $K = 2.5$ W m^{-1} K^{-1}), together with the 20 K km^{-1} gradient in the absence of convection, the permeability must exceed $\sim 1 \times 10^{-14}$ m^2. This value lies towards the lower end of the 10^{-11} to 10^{-15} m^2 range expected by analogy with the Earth, and could be taken to imply that convection did not extend through the full vertical extent of typical aquifers. In contrast, if the much larger permeabilities suggested by the high discharges are correct then convection would easily occur throughout all aquifers. If convection does occur, it effectively increases the thermal conductivity of the aquifer, probably by a factor of two, based on simulations of volcanic intrusions producing hydrothermal systems (Ogawa *et al.*, 2003). This conclusion reduces the temperature gradient across the aquifer and acts to decrease the average water temperature, also by a factor of two, which would lead to a mean water temperature of about 30 °C in a 5 km thick aquifer. However, the temperature gradient is also one of the factors determining the critical permeability, and reducing the temperature gradient increases the minimum permeability that allows convection. Thus, to some extent the process is self-limiting, and without explicit knowledge of the actual permeabilities of aquifers on Mars it is difficult to do any better than to assert that aquifer water temperatures may lie in the range from just above the (weakly pressure- and hence depth-dependent) freezing point to at least 30 °C.

Reduction of the water temperature during its ascent will occur by two processes: adiabatic decompression and conduction through the fracture walls. The adiabatic temperature change ΔT_r of water rising a vertical distance $H = 6$ km through the crust, assuming a near-lithostatic pressure distribution in the water so that the excess pressure due to the water buoyancy drives the water motion, can be expressed as

$$\Delta T_r = (\alpha_w T_r g \rho_r H)/(c_w \rho_w), \quad (16.2)$$

Table 16.2. Conductive cooling of water rising in fractures

Fracture width W (m)	Rise speed U (m s^{-1})	Transit time τ (s)	Conductive cooling ΔT_c (K)
0.1	9.7	410	34.7
0.3	16.9	237	8.8
1.0	30.8	130	2.0
3.0	53.4	75	0.5

Note: Pressure gradients specified in text.

where T_r is the average water temperature and ρ_r is the density of the crust, $\sim$3000 kg m^{-3}. Using values relevant to the water having a temperature somewhere in the range 0–30 °C ($\alpha_w = 2.5 \times 10^{-4}$ K^{-1}, $T_r = \sim 300 \pm 25$ K, $c_w = 4180$ J kg^{-1} K^{-1} and $\rho_w = \sim 1000$ kg m^{-3}) we find that ΔT_r will be only 1.2 K.

Cooling by conduction of heat into the walls of the fracture through which water rises may be more important. The speed U of the water in a fracture of width W, the motion being fully turbulent in all cases of interest, is given by

$$U = [(W\,\mathrm{d}P/\mathrm{d}z)/(f\rho_w)]^{1/2}, \tag{16.3}$$

where f is a wall friction factor of order 10^{-2} and $\mathrm{d}P/\mathrm{d}z$ is the pressure gradient driving the motion. At the onset of water release, the pressure gradient will be the sum of contributions due to the buoyancy of the water relative to the crust, $g(\rho_r - \rho_w) = 7440$ Pa m^{-1}, and any excess pressure in the aquifer. Excess pressure may arise due to a topographic gradient in the aquifer (Head *et al.*, 2003a), due to tectonic pressurisation of the crust (Hanna and Phillips, 2006), or due to downward growth of the base of the cryosphere as the planet cools and the geothermal gradient decreases (Wang *et al.*, 2006). A topographic height difference of $Z = 2$ km, common in the highland areas of Mars (Neumann *et al.*, 2004) underlain by aquifers, would yield an excess pressure of $(\rho_w g Z) = 7.4$ MPa, similar to the 10 MPa tectonic excess pressures found by Hanna and Phillips (2006), implying an excess pressure gradient over the vertical extent of the fracture $D = \sim$3.5 km of 2100 Pa m^{-1}. Combined with the pressure gradient due to buoyancy, this gives a total pressure gradient of 9500 Pa m^{-1}. This results in the water rise speeds as a function of fracture width shown in Table 16.2. Also given are the transit times, τ, of any given batch of water. The transit time controls the amount of heat lost by the water. At a time t after the opening of the fracture, a wave of warming will have penetrated a distance $\lambda = \sim(\kappa t)^{1/2}$ into the surrounding crust, where κ is the thermal diffusivity of cryosphere material, about 7×10^{-7} m^2 s^{-1}. The crustal temperature gradient controlling heat flow away from the fracture will then be $\mathrm{d}T/\mathrm{d}x = (T_r - T_c)/\lambda$, where T_r and T_c are the mean water and cryosphere temperatures. If T_c is 240 K, a conservative value of T_r would be 300 K. Consider a fracture of horizontal length L; the total instantaneous heat flux out of the two faces of the fracture is $(2KDL\,\mathrm{d}T/\mathrm{d}x)$, and so the heat lost during the transit time τ will be $(2\tau KDL\,\mathrm{d}T/\mathrm{d}x)$. The mass of water losing this heat is equal to $(\rho_w WLD)$, and so the temperature decrease in the water, $\delta T(t)$, will be equal to $[2\tau K(T_r - T_c)]/[\rho_w W c_w(\kappa t)^{1/2}]$. The average value of the temperature reduction, ΔT_c, due to conductive heat loss during the travel time, τ, of a given batch of water through the fracture is equal to $(1/\tau)\int \delta T(t)\,\mathrm{d}t$. For the first batch of water rising through the fracture, for which heat loss is at a maximum because there has been no pre-heating of the fracture walls, the integral is to be evaluated between $t = 0$ and $t = \tau$, and is found to be

$$\Delta T_c = [4\tau^{1/2} K(T_r - T_c)]/[\rho_w W c_w \kappa^{1/2}]. \tag{16.4}$$

Table 16.2 shows the values of ΔT_c; clearly, even the initial conductive losses are small for fracture widths in excess of one metre, and all conductive losses decrease with time as the fracture walls are progressively heated. For comparison, using various arguments to select the pressure gradient, Head *et al.* (2003a) found $W = 2.4$ m and $U = 64$ m s^{-1} for the fractures in the Cerberus Fossae graben system feeding the Athabasca Valles, and Manga (2004) found values of W up to 2 m implying U was up to $\sim$40 m s^{-1} for the same system. These results would imply transit times of order 60–100 s and water temperature decreases of less than 0.5 K. These minimal heat losses during ascent imply that the temperature of water emerging at the surface of Mars may lie in the range from just above the freezing point to about 30 °C.

16.4 Water release at the surface

In lieu of other factors, a rise speed U of up to $\sim$50 m s^{-1} implies that water reaching the surface of Mars through a fracture may be expected to form a fountain over the release site with a height of $U^2/(2g)$, in excess of 300 m. However, the issue may be more complicated if the water contains dissolved volatile compounds that come out of solution as the low ambient pressure at the surface is approached. Stewart and Nimmo (2002) use thermodynamical arguments to show that it is extremely unlikely that subsurface water on Mars will contain significant carbon dioxide (CO_2) derived from the atmosphere. However, in the case of a water-release event triggered by a volcanic intrusion, it is possible that CO_2 released from an intrusion might migrate into the aquifer as it was expelled from the cooling magma. The geometry would be particularly favourable for this if the intrusion were a sill. By analogy with Earth, a mafic mantle-derived magma could contain

a CO_2 mass fraction as large as 0.0065 (Gerlach, 1986). If this magma was emplaced as a sill at the base of an aquifer at a depth of 10 km, where the ambient pressure is 120 MPa (the sum of a lithostatic pressure of 112 MPa and an excess water pressure of 7 to 10 MPa), the solubility of CO_2 in mafic magma (Harris, 1981; Dixon, 1997) is such that most of this CO_2 would be exsolved from the magma and would percolate up into the aquifer water where it would readily be dissolved. Taking plausible thicknesses of sills (about 200 m, Leask *et al.*, 2006c) and aquifers (6 km, see above) and of the volume fraction of an aquifer occupied by water (5%, based on the Mars crustal porosity model of Hanna and Phillips, 2005), the CO_2 would represent a mass fraction in the water of ∼0.01 (Bargery and Wilson, submitted).

This amount of CO_2 would readily dissolve in the water at the base of the aquifer (Diamond and Akinfiev, 2003) and, furthermore, would still be retained if convection carried water to the top of the aquifer where the pressure is about 55 MPa. However, when fracturing of the overlying cryosphere allowed the water to ascend to the surface, essentially all of this CO_2 would be exsolved. A model (Bargery, 2007), analogous to the treatment of CO_2 release in overturning lake water (Zhang and Kling, 2006), of the progressive release of the gas to form bubbles as the water nears the surface shows that the volume fraction of CO_2 gas in the ensuing foam would reach 0.8, leading to foam collapse, at a depth of 10 m. Expansion of the CO_2 from the pressure at this depth to atmospheric pressure would provide 2600 J kg^{-1} of energy to add to the kinetic energy of the rising water before gas release, thus increasing the water emergence speed from a likely maximum (without dissolved CO_2) of 50 m s^{-1} to a maximum of 90 m s^{-1}. This increase in velocity would lead to formation of a fountain more than 1000 m high (Bargery, 2007). It should be stressed, however, that events like this may be rare, associated only with water release from areas of sill-related chaos, and that fountain heights up to about 300 m from fractures induced by dyke intrusions are likely to be more common.

The water at the outer edge of a fountain is exposed to an environment where the ambient temperature is on average 210 K (though it may, on rare occasions at the equator in the southern hemisphere summer, exceed 273 K) and the atmospheric pressure is 600 Pa at the mean surface elevation, 700 Pa in low-lying areas, 200 Pa on the flanks of large shield volcanoes and as little as 70 Pa at some of their summits. The triple point of pure water is at 273.15 K and 610.7 Pa and the vapour pressure increases rapidly with temperature (Figure 16.1). Given the estimates from the previous section of released water temperatures in the range from a few °C to 30 °C, i.e., 275 to 300 K, Figure 16.1 implies that, initially at least, vigorous evaporation of the water forming the outer envelope of the fountain will take place at all but the lowest elevations. The resulting vapour will expand and cool, ultimately reaching the surface in the solid form in a zone around the base of the liquid fountain. This process will be rendered less vigorous if aquifer water on Mars contains dissolved salts (e.g. Burt and Knauth, 2003), because these will reduce the vapour pressure at a given temperature and reduce the freezing point temperature. Nonetheless, geomorphological evidence indicates that this process may have occurred at the Mangala Valles fissure-headed outflow channel, where a restricted area of ridges and lobes on the rims of the source graben has been interpreted as moraines and tills deposited by locally derived ice and snow (Head *et al.*, 2004). The formation mechanism for this ice and snow is suggested to have been the rising and flooding by groundwater of the source graben, boiling and freezing of this ponded water, sublimation, and redeposition in solid form on the fissure rim. As discussed here, an alternative explanation for the formation of these features is through water vapour production at the outside of a water fountain, radiative cooling of the vapour to solid form, and deposition of this material on the surface as snow or ice. The first scenario is taken to imply that the Hesperian–Amazonian climate during formation of these moraine and till features was a hyper-arid cold desert similar to the climate of Mars today (Head *et al.*, 2004). The alternative scenario does not hold any implications about the palaeoclimate, but contains information about the depth and temperature of the

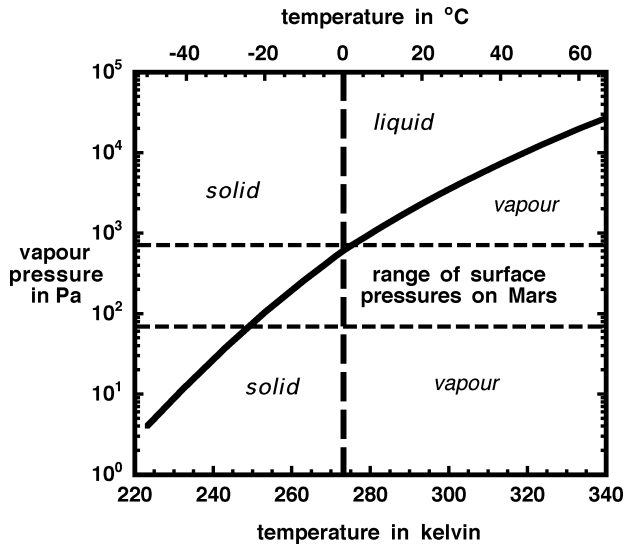

Figure 16.1. Variation of the vapour pressure (solid curve) of pure liquid and pure solid H_2O with temperature. The long-dashed line indicates the solid–fluid boundary and crosses the vapour pressure curve at the triple point, at 273.15 K and 610.7 Pa. The range of surface atmospheric pressures between low-lying plains and volcano summits on Mars is indicated by the short-dashed lines.

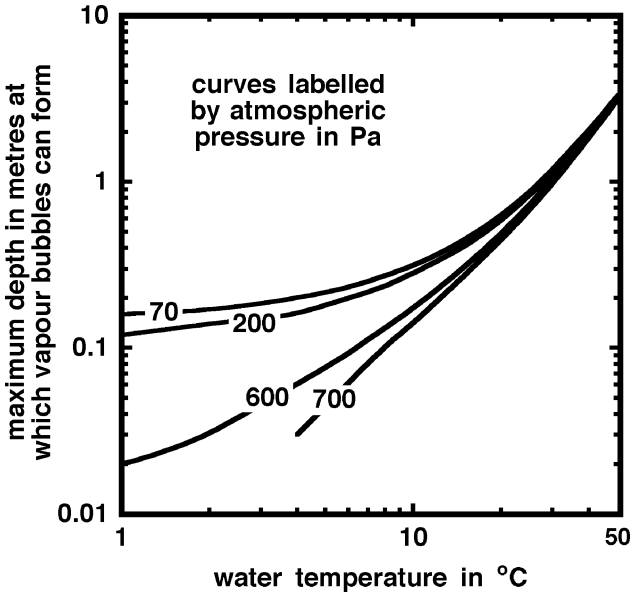

Figure 16.2. Values of the maximum depth at which water vapour bubbles form in a sheet of water as a function of the temperature at which it is released onto the surface of Mars and the ambient atmospheric pressure. Pressures of 700 and 600 Pa correspond to common elevations near Mars datum. Pressures of 200 and 70 Pa correspond to the flanks and summits, respectively, of large shield volcanoes. The absence of part of the 700 Pa curve indicates that no significant boiling occurs.

groundwater aquifer and the processes upon water release. The lack of observation of similar moraine and till features around other fissure-headed outflow channels that formed in the late Amazonian (Burr *et al.* this volume Chapter 10), during a cold climate conducive to glaciation (Neukum *et al.*, 2004) or of the formation of multi-layered surficial ice deposits (Head *et al.*, 2003b), suggests that climatic influence is not the controlling factor in the formation of these features.

Evaporation of water flowing away from a fountain will continue as long as the water remains warm enough for its vapour pressure to exceed the atmospheric pressure. Vapour bubbles will form in the water and rise up to burst at the surface. Using the temperature dependence of the vapour pressure (Kaye and Laby, 1995), the maximum depths below the surface at which vapour bubbles would form at various elevations are calculated and hence ambient pressures on Mars for a range of water release temperatures are derived, assuming that the overlying fluid is water with a density of 1000 kg m^{-3} (Figure 16.2). However, these are minimum estimates of these depths because in practice the fluid will be a mixture of liquid and vapour with a significantly smaller bulk density, so the actual depths of bubble nucleation may be greater than those given by a factor of up to 10.

The significance of water evaporation, whether by boiling or diffusion into the atmosphere, for subsequent water flow across the surface will be a function of the way the water cools. Cooling in turn will be influenced by the latent heat removed by the evaporation process itself and by the sensible heat lost to heating ice and silicates in cryosphere material eroded from the bed of the channel and entrained into the flow. These issues are addressed later, but first the basic dynamics of water flow in channels is considered.

16.5 Dynamics of water flow

16.5.1 Basic relationships governing water flow

The most important parameters determining the dynamics of water flow in channels on planetary surfaces are the bed slope α, the bed roughness, and the water depth d. If the width, w, of a channel is comparable to the depth, the influence of the banks cannot be neglected and, in general, the dimensions must be characterised by the hydraulic radius of the channel, R, defined as the cross-sectional area of the channel divided by its wetted perimeter, i.e.

$$R = (wd)/(w + 2d). \tag{16.5}$$

However, if w is much greater than d, as is commonly the case for large-scale natural water channels in general and for the Martian outflow channels in particular, then R is essentially equal to d.

Various equations are available to relate the above parameters to the mean water flow speed, u. The earliest is that due to Manning (1891); writing $S = \sin \alpha$, this relationship is

$$u = (R^{2/3} S^{1/2})/n, \tag{16.6}$$

where n is the Manning coefficient, a parameter with the dimensions of time divided by length$^{1/3}$, that characterises the combined effects of bed roughness, bed form and reach geometry. This equation, like a similar one due to Chézy (Herschel, 1897), has the disadvantage that it was developed for application only to the Earth, and does not explicitly account for the effects of the acceleration due to gravity, g. Various authors have attempted to use this equation for Martian channels by correcting for the differing values of g between Mars and Earth (see summary in Wilson *et al.*, 2004) but, even when done correctly, this leaves a residual problem. Gioia and Bombardelli (2002) showed that, in addition to the effects of gravity, the Manning coefficient involves a length scale that represents the typical physical scale of bed roughness. Thus, even when the differing gravities are accounted for, use of the resulting Manning coefficient may not be appropriate for Mars unless the bed roughness in Martian outflow channels is generally similar to that in the terrestrial rivers from which values of the

Manning coefficient are derived. Wilson *et al.* (2004) used the treatment of Gioia and Bombardelli (2002) to derive recommended values of the Manning coefficient for Martian channels, but also recommended against use of the Manning equation in favour of the treatment that follows.

A more fundamental relationship between the variables can be derived from dimensional analysis, the Darcy–Weisbach equation (ASCE, 1963):

$$u = [(8gRS)/f_c]^{1/2}, \tag{16.7}$$

in which f_c is a dimensionless friction factor that depends on the bed roughness relative to the flow depth for a given bedform. The friction factor plays the role of converting the shear velocity of the flow, $(gRS)^{1/2}$, to the average flow velocity. Equation (16.7) is applicable to fluid flows in channels and pipes of any cross-sectional shape provided that R is defined correctly. However, it should be noted that in some engineering applications a factor of two is adopted, rather than the value eight appearing in the above expression, leading to correspondingly smaller values for the friction factor. Bathurst (1993) gave relationships, based on a large body of experimental and field data, for the variation of f_c with bed roughness and water depth for a wide range of bed particle sizes and bedforms. In the case of channels with sand beds, Bathurst (1993) gave implicit expressions for f_c, and Wilson *et al.* (2004) manipulated these to yield the explicit formulae given as Equations (16.8) and (16.9) below. Equations (16.10), (16.11) and (16.12) are taken directly from Bathurst (1993). Equation (16.13) is adapted from engineering data on fluid flow in rough pipes (Knudsen and Katz, 1958) as a proxy for channels with fixed bed roughness. Finally, Equation (16.14) is a recent fit to a wide range of data from various sources given by Kleinhans (2005).

Channels with sand-dominated beds There are two main regimes for flow in channels with beds dominated by sand-size material (Hjülstrom, 1932): a lower regime (plane bed with sediment transport, or bed with ripples and dunes) and an upper regime (bed with sediment transport having antidunes and chutes and pools). A transition zone between these two regimes may have bedforms transitional between dunes and antidunes. Resistance formulae may take account separately of grain drag and bedform drag or combine the two together. The combined formulae are

$$(8/f_c)^{1/2} = 4.529(R/D_{50})^{0.02929} S^{-0.1113} \sigma_g^{-0.1606} \quad \text{lower regime,} \tag{16.8}$$

$$(8/f_c)^{1/2} = 7.515(R/D_{50})^{0.1005} S^{-0.03953} \sigma_g^{-0.1283} \quad \text{upper regime,} \tag{16.9}$$

where D_{50} is the channel-bed clast size such that 50% of clasts are smaller than D_{50} and σ_g is the geometric standard deviation of the bed clast size distribution, a dimensionless number equal to the ratio of the mean size to the size one standard deviation away from the mean.

Channels with gravel-dominated beds If the channel bed is dominated by gravel-size clasts, the grain size of the bed material is characterised by the parameter D_{84}, the channel-bed clast size such that 84% of clasts are smaller than D_{84}. Account is also taken of irregularities in channel depth by including the maximum channel depth d_m such that

$$(8/f_c)^{1/2} = 5.75 \log_{10}[(d_m^{0.314} R^{0.686})/D_{84}] + 2.8822. \tag{16.10}$$

Channels with boulder-dominated beds The relationship is

$$(8/f_c)^{1/2} = 5.62 \log_{10}[R/D_{84}] + 4. \tag{16.11}$$

Steep channels with fall and pool structures Steep channels on hillsides exist on Mars but these are generally very much smaller features than the outflow channels; however, the relevant formula is included here for completeness. The grain size of the bed material is incorporated via the parameter D_{90}, the channel-bed clast size such that 90% of clasts are smaller than D_{90}. Also, because all bed material is assumed to be constantly in motion, the depth parameter used is d_s, defined as the total depth of water plus sediment. The relationship is

$$(8/f_c)^{1/2} = 5.75\{1 - \exp[(-0.05d_s)/(D_{90}S^{1/2})]\}^{1/2} \times \log_{10}[(8.2d_s)/D_{90}]. \tag{16.12}$$

Channels with fixed bed roughness The following function, taken from engineering data on fluid flow in rough tubes (Knudsen and Katz, 1958), is included to characterise channels in which the bed roughness elements are fixed and cannot be moved by the fluid. Such conditions might arise if a channel previously created by an energetic outflow was re-used by a later, less energetic event. If r is the typical size of bed roughness elements (probably to be equated with D_{50}), then

$$(8/f_c)^{1/2} = 5.657 \log_{10}[R/r] + 6.6303. \tag{16.13}$$

Large terrestrial data set Kleinhans (2005) drew attention to the large uncertainties associated with relating friction factors of bed roughness and suggested the following function based on data relating to 190 water channels on Earth, including sand-bedded rivers with dune beds and 10 channels created by catastrophic glacial outburst events:

$$(8/f_c)^{1/2} = 2.2(R/D_{50})^{-0.055} S^{-0.275}. \tag{16.14}$$

Table 16.3. Morphological properties of outflow channels relevant to water discharge rates

Valley	Tangent of regional slope	Tangent of floor slope	Channel width (km)	Channel depth (m)
Athabasca	0.0004	0.0003	15–25	~100
Grjotá	0.0008	0.0006	several tens	~10
Mangala	0.0008	0.0005	~35 (proximal)	20–100
Marte	0.0003	0.0002	several tens	a few tens
Ravi	0.0050	0.0025	~20	~500

16.5.2 Morphological characteristics of outflow channels relevant to water flow speeds

Outflow channels on Mars have formed in regions where the large-scale topographic slopes have values of $\tan \alpha$ ranging from 3×10^{-4} to 5×10^{-3} (Wilson *et al.*, 2004; Burr *et al.*, this volume Chapter 10; see Table 16.3). As these channels developed by bed erosion, it appears that generally they were deepened most extensively in their proximal parts (though there are some exceptions dictated by very non-uniform preflood topography – see Burr *et al.*, this volume Chapter 10). Preferential proximal erosion is to be expected for two reasons. Firstly, particles removed from the bed by erosion must be transported by the water, and so the fraction of the moving fluid that consists of entrained solids increases with distance from the source up to some limiting value. Because the water must share its momentum with the entrained material, the entrained sediment acts to reduce the velocity and modify the turbulence regime in the water-sediment mixture and to reduce the erosion rate (Gay *et al.*, 1969). Indeed, if the bedload becomes large enough such that the flow is hyperconcentrated, the rheology of the fluid will cease to be Newtonian (Bargery *et al.*, 2005). The fluid then effectively becomes a mud flow or lahar, and will become depositional (Carling *et al.*, this volume Chapter 3). The issue of whether and how a flow may become hyperconcentrated is discussed later. Secondly, most of the surfaces into which outflow channels were incised on Mars probably consisted of cryosphere (Clifford, 1993), a mixture of very cold (e.g. 210 K) ice and rock in the volume proportions of 1 to 4, or 1 to 5 (Hanna and Phillips, 2005). Part of the erosion process included the melting of the ice component, and the sensible and latent heat required for this was extracted from the flowing water, causing progressive cooling with a consequent reduction in the down-flow ice-melting potential (Bargery *et al.*, 2005). Eventually ice crystal formation began, with the ice crystal volume fraction competing with silicate sediments for the carrying capacity of the remaining water. The net effect of the variation in bed erosion rate with distance from source has been to produce channels whose floors slope at values less than the local pre-erosion regional slopes: floor slope values are generally in the range 2×10^{-4} to 2×10^{-3} (Table 16.3).

Although no spacecraft has visited the floor of a Martian outflow channel, the Viking and Pathfinder spacecraft landed on geological units that may consist at least in part of materials washed through outflow channels (Golombek *et al.*, 1997), and so the rock size distributions on the surfaces at the Viking 1 and 2 and Pathfinder landing sites may be used as proxies for the size distributions of clasts in such channels. Using the data measured at these sites (Golombek and Rapp, 1997; Golombek *et al.*, 2003), Wilson *et al.* (2004) derived values for typical clast size distribution functions. Kleinhans (2005) has pointed out the need for a correction to the analysis of Wilson *et al.* (2004). Taking account of this, the values of the parameters of the bed clast size distribution needed for Equations (16.8) to (16.14) can be approximated as $D_{50} = 0.1$ m, $D_{84} = 0.48$ m, $D_{90} = 0.6$ m and $\sigma_g = 2.9$, respectively.

The depths of outflow channels commonly lie in the range 20 to 500 m (Table 3), though Smith *et al.* (1998) give depths up to 1300–1600 m for Ares Vallis. However, there have been significant differences of opinion in the literature about the depth of the water that typically flowed in these channels. Some authors have tacitly assumed that channels were always bankfull, though this is extremely unlikely for the following reason. It is clear that there was extensive, progressive erosion of the channel floors. Assume first that the erosion rate was constant. If a channel remained full, the water depth would have increased linearly with time. Equation (16.7) shows that the water flow speed would have increased as the square root of the depth and hence as the square root of the time. The volume flux, F, flowing through a channel of width w and depth d at speed u is

$$F = wdu, \tag{16.15}$$

so that F would also have had to increase with time. Even if the sides of the channel were vertical, so that the water did not get wider as it got deeper, the volume flux would have had to increase as time to the power $3/2$. If, instead of being constant, the bed erosion rate increased, say linearly, with

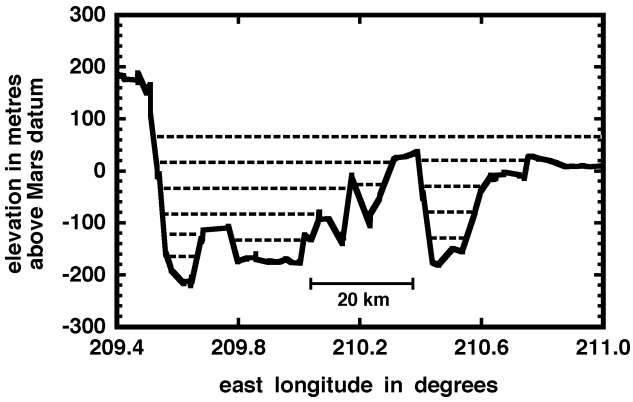

Figure 16.3. Cross-sectional profile at right-angles to water flow direction in Mangala Valles at 16.7° N using unsmoothed MOLA data. The presence of subvalleys on the floor of the main valley is clear, and the consequences of progressive water depth increases in ∼50 m increments from the floors of each of these subvalleys is illustrated. It is inferred that water depths were ∼50–100 m for most of the duration of the valley-forming event. (Based on Figure 9 in Leask *et al.* (2007); copyright (2007) American Geophysical Union.)

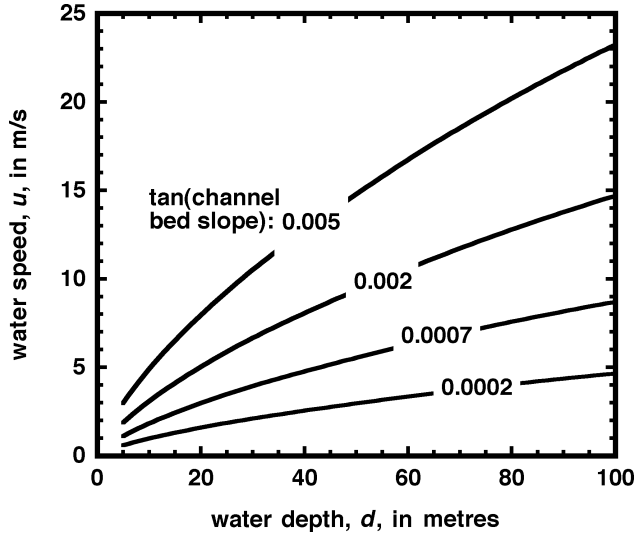

Figure 16.4. Variation of mean water flow speed, u, with water depth, d, in a channel on Mars for four values of the tangent of the channel-bed slope. At slopes this shallow, the tangent of the slope is essentially identical to the sine of the slope.

the flow speed, then F would have had to increase as time cubed. In practice, all reasonable scenarios for subsurface water release involve a rapid rise to a maximum discharge with a subsequent decline (Andrews-Hanna and Phillips, 2007), often roughly exponential (Manga, 2004). Thus we think it very likely that, for most of the time of their formation, the water levels in most of the channels were only a small fraction of the final channel depths, thus technically making these features valleys rather than channels, though we retain the latter term for consistency. This is underlined by the observation that, whereas the total widths of channels are commonly in the range 10 to 30 km (De Hon and Pani, 1993), channel floors are generally not flat but instead consist of a small number of subchannels with widths in the range 5–10 km. The depths of these subchannels are mainly in the range 10 to 50 m (e.g. Figure 16.3), and it may be inferred that values in this range are much better estimates of maximum water depths.

16.5.3 Water flow speeds and predicted discharge estimates

In a wide-ranging survey of possible modes of fluvial sediment transport and deposition on Mars, Kleinhans (2005) has suggested that the size distribution of the clasts moving through many Martian fluvial systems may have been distinctly bimodal, with roughly equal proportions of silt/sand and coarse gravel/cobbles. Given that the concern here is with large outflow channels, it is tacitly assumed to have involved short-lived catastrophic events involving energetic bed erosion, and so it is logical to use Equation (16.11) for channels beds dominated by boulders in generating values for friction factors, with the grain size parameters derived from the Viking and Pathfinder landing sites ($D_{50} = 0.1$ m, $D_{84} = 0.48$ m, $D_{90} = 0.6$ m and $\sigma_g = 2.9$). Combining the above maximum water depths (10–50 m) and channel-bed slope estimates ($\tan\alpha = 2 \times 10^{-4}$ to 2×10^{-3}), a range of likely maximum water flow speeds are derived as a function of water depth. These are shown in Figure 16.4; at each water depth the speed is given for each of four channel-bed slopes, 0.0002, 0.0007, 0.002 and 0.005. The three smallest of these span the range found for channel floors, and the largest represents a likely upper limit for pre-channel topography. Clearly, for mature channels that have reached their final floor slope, water flow speeds should lie mainly in the range 3 to 10 m s^{-1} if water depths do not exceed 50 m, and could be up to 15 m s^{-1} if water depths range up to 100 m. Unfortunately, there is no obvious way of estimating likely water depths on pre-channel topography, though Leask *et al.* (2006a) used the outermost terraces on the walls of Ravi Vallis to estimate an early-stage channel depth of at most 50 m on an unusually steep terrain slope of $\tan\alpha = \sim 0.01$; this implies a water speed of about 21 m s^{-1}. The range of water speeds is consistent with the sizes of clasts observed at the Viking and Pathfinder landing sites: flow speeds of order 10 m s^{-1} would be readily able to transport clasts approaching a metre in size (see Figure 16.7 in Kleinhans, 2005).

Using the observation that main channels are commonly 10–30 km wide and contain a small number of subchannels with widths in the range 5 to 10 km, an estimate of likely total channel discharges is obtained by combining the flow speeds in Figure 16.4 with a typical total

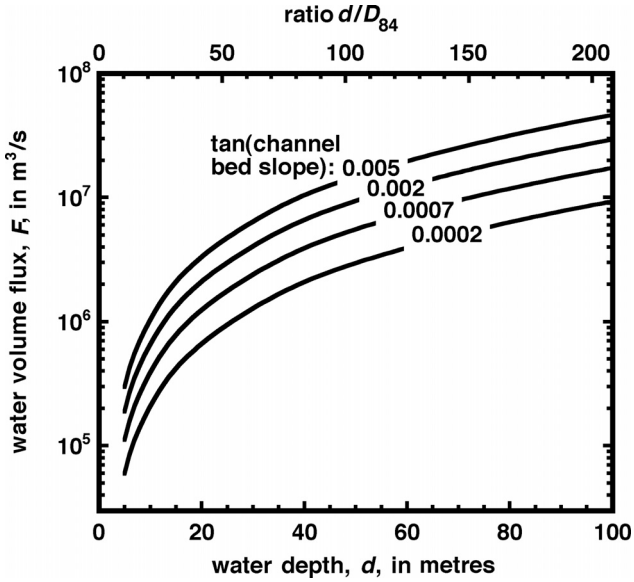

Figure 16.5. Water volume flux, F, as a function of water depth, d, on Mars in steep-sided channels 20 km wide, for four values of the tangent of the channel-bed slope. The volume flux is directly proportional to the channel width. The upper axis gives values of the water depth, d, divided by the bed roughness scale, D_{84}, to aid comparison with other channel systems.

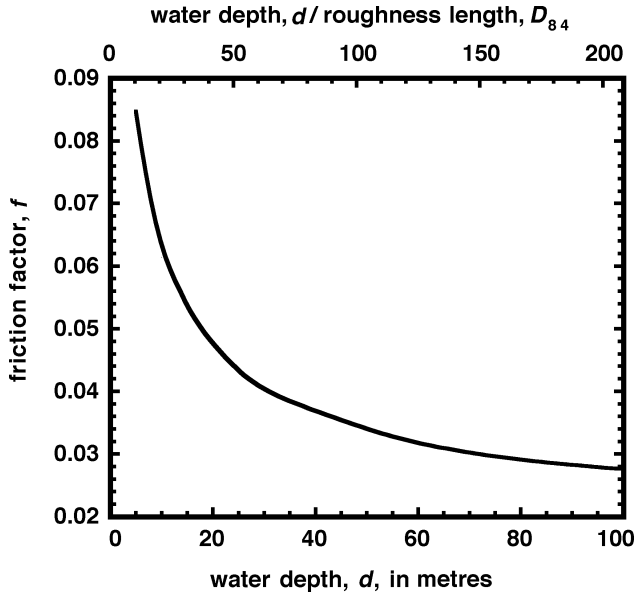

Figure 16.6. Bed friction factor, f, as a function of water depth, d, in channels on Mars in which the bed roughness is dominated by boulders, so that the friction factor is independent of bed slope. The upper axis shows the ratio of water depth to roughness scale, D_{84}, so that these results can be scaled to other roughness parameters.

active flowing water width of 20 km. This results in the variation of volume flux with water depth and bed slope given in Figure 16.5: fluxes in the range 10^5 to about $3 \times 10^7\,\mathrm{m^3\,s^{-1}}$ should have been common. These values are comparable to the smaller flux estimates summarised in Table 16.1.

16.5.4 Subcritical or supercritical flows?

An important parameter controlling the state of a fluid flow is its Froude number, *Fr*. Froude numbers in excess of unity correspond to highly unsteady, supercritical flow conditions, and fluids forced to flow under supercritical conditions commonly undergo hydraulic jumps after they have flowed for a short distance, with an increase in water depth and a decrease in velocity, in order to reduce the Froude number to less than unity. These flows also erode their beds over time in a way that reduces the bed slope so that the supercritical conditions are avoided (e.g. Grant, 1997; Hunt *et al.*, 2006). Froude number is defined by

$$Fr = u/(gd)^{1/2}. \tag{16.16}$$

Equation (16.16) can be combined with Equation (16.7) giving the flow speed in terms of the physical variables to yield

$$Fr = [(8 \sin \alpha)/f_c]^{1/2}. \tag{16.17}$$

If Equation (16.11) is used for the friction factor in channels with beds dominated by boulders, f_c is independent of channel-floor slope and is only a function of water depth; the relationship is shown in Figure 16.6. For a 50 m deep water flow, f_c is 0.034. Thus for floor slopes of $\tan \alpha = 0.0002$, 0.0007 and 0.002, the range spanning mature channel floors, the implied Froude numbers are 0.22, 0.41 and 0.69, respectively, all values being subcritical. For a 100 m water depth the friction factor is 0.0276 and the corresponding Froude numbers for mature channels are 0.24, 0.45 and 0.76, again all subcritical values. However, for a pre-erosion topographic slope as steep as $\tan \alpha = 0.005$, the value measured in the case of Ravi Vallis (Table 16.3), the Froude numbers for 50 and 100 m water depths would have been 1.08 and 1.20, respectively, both supercritical values. All of these results are summarised in Figure 16.7; they lend support to the idea that the outflow channels developed in ways that tended to reduce their bed slopes and so eliminate potentially supercritical conditions that may have been present in the early stages of their formation, a process observed to operate in driving the development of the flow regimes in rivers on Earth (Grant, 1997; Kleinhans, 2005).

The most common bedforms observed in the Martian outflow channels are streamlined forms, which provide only imprecise information regarding flow conditions (see Carling *et al.*, this volume Chapter 3). However, observations of inferred subaqueous dunes support the idea from

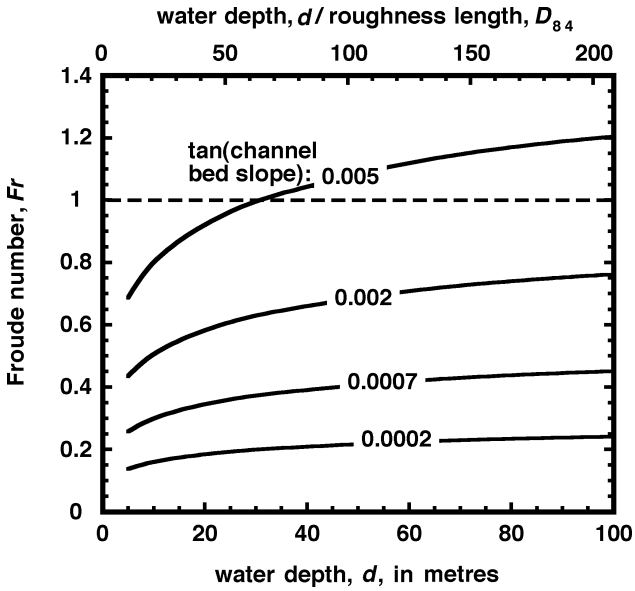

Figure 16.7. Froude number, *Fr*, as a function of water depth, *d*, in channels on Mars in which the bed roughness is dominated by boulders, for four values of the tangent of the channel-bed slope. As in Figure 16.5, the upper axis shows the ratio of water depth to roughness scale D_{84}. The horizontal broken line marks the transition between sub- and supercritical flow at $Fr = 1$.

the analysis above that flow in Martian outflow channels tends toward subcritical conditions. Dunes in plan-view morphology are elongate features oriented transverse to the direction of flow. Topographically, dunes are asymmetric, having a more shallowly sloping stoss (upstream) side and a more steeply sloping lee (downstream) side, which results from the difference in stoss and lee deposition processes (see Burr *et al.* (2004) or Carling *et al.*, this volume Chapter 3, for further description and explanation of dune formation). Subaqueous dunes have been identified in Athabasca (Burr *et al.*, 2004) and Maja Valles (Chapman *et al.*, 2003). The features observed in Maja Valles were classified as subaqueous dunes on the basis of their plan-view similarity to dunes in Jökulsá á Fjöllum, a Holocene-aged outflow channel in northern Iceland (Waitt, 2002). The transverse bedforms in Athabasca Valles were classified as dunes on the basis of their plan-view morphology and also their asymmetric vertical shape, which was similar to that observed for subaqueous dunes in Pleistocene-aged flood channels in the Altai Mountains of Siberia (Carling, 1996). In contrast to dunes, antidunes form within high subcritical (i.e., trans-critical) or supercritical flow (Fr > 1). Bedforms in one outflow channel have been proposed to be antidunes (Rice *et al.*, 2003), but the 3D morphology of the field of bedforms was found to be inconsistent with an antidune classification, and a duneform interpretation is preferred (Burr *et al.*, 2004).

16.5.5 Bed erosion

The great depths (tens to perhaps a hundred metres) of the Martian outflow channels imply an efficient bed erosion process. Baker (1979) discussed processes responsible for eroding the Missoula Flood channels on Earth and suggested the possible importance of cavitation – the production and collapse of vapour bubbles when transient velocity changes due to the presence of irregularities on the bed of a channel cause the local pressure to decrease below the saturation vapour pressure of the water. Baker (1979) used an analysis proposed by Barnes (1956). Re-deriving the equations of Barnes in their most general form, the following expression is derived for the mean flow speed u that, when increased locally by a factor Φ, will cause cavitation in a flow of depth d:

$$u = [2/(\Phi^2 - 1)]^{1/2}\{[(P_a - P_v)/\rho_w] + gd\}^{1/2}, \quad (16.18)$$

where P_a is the atmospheric pressure, P_v is the saturation vapour pressure of the water (a function of the water temperature) and as before ρ_w is the water density. The vapour pressure of water near its freezing point is comparable to the Martian atmospheric pressure, 600 Pa, whereas at 30 °C it is 4.2 kPa. Thus, depending on the temperature of the water as it is released and how much cooling it has undergone, $(P_a - P_v)$ could range from 3.5 kPa to a few tens of Pa. Then the term $[(P_a - P_v)/\rho]$ would range from 3.5 $m^2\,s^{-2}$ to 0.1 $m^2\,s^{-2}$. Above it has been argued that water depths in Martian channels are likely to be 10–50 m, so the value of (gd) will be 40–200 $m^2\,s^{-2}$, almost always dominating the second term in the above equation. Inserting the smallest likely value for $[(P_a - P_v)/\rho]$, 0.1 $m^2\,s^{-2}$, and corresponding pairs of values of u and d from Figure 16.4, it is found that for cavitation to occur would require Φ to be at least ~3.0 for $u = 3\,m\,s^{-1}$, $d = 10\,m$, and to be at least ~2.2 for $u = 10\,m\,s^{-1}$, $d = 50\,m$. Barnes (1956) asserted that obstructions on a stream bed on Earth could locally double the fluid velocity, i.e. cause $\Phi = 2$, and there is no reason why a similar argument should not hold for Mars. Thus, at least for the deeper, faster-flowing floods, cavitation should generally have been as effective a source of bed erosion in outflow channels on Mars as it has been suggested to have been on Earth. Equation (16.18) implies that the minimum value of Φ required to allow cavitation to occur increases as the flow speed decreases. Flow depth and hence flow speed are likely to decrease with distance from the point of release of a water flood on Mars due to both water vapour loss and momentum transfer to transported sediment. Thus if enhanced bed erosion is caused by cavitation it is likely to be greatest nearest the water release point, thus encouraging channels to decrease in depth with distance from source, as is observed generally. It is also possible that the erosion caused by cavitation would remove the bed irregularities increasing the flow speed, thus implying that the process

would act preferentially in the early stages of channel formation.

16.5.6 Water volumes and event durations

Various authors (e.g. Komar, 1979; Ghatan *et al.*, 2005; Leask *et al.*, 2006a, 2007) have assumed that a minimum value for the volume of water passing through a Martian channel system can be found by estimating the volume of crustal material eroded and assuming that the floodwater carried some maximum sediment load, generally taken to be about 30–40% by volume. The volume V_s of cryosphere material eroded from a channel can be assessed from topographic profiles constructed using laser altimeter data from the Mars Orbiter Laser Altimeter on Mars Global Surveyor by making some simple plausible assumptions about the pre-erosion topography. If the mixture of water and eroded solids contains a volume fraction Q of solids, then the water volume V_w is equal to $[(1 - Q)/Q]V_s$, and with Q in the range 0.3 to 0.4, V_w will be 1.5 to 2.3 times the estimated missing cryosphere volume. Furthermore, dividing the water volume V_w by the water discharge-rate estimate for the same channel yields the minimum duration of the water release event. Using this method, Leask *et al.* (2006a) estimated that a total of a little more than 8000 km^3 of cryosphere was eroded from the Ravi Vallis–Aromatum Chaos system due to a water release rate averaging $\sim$10 to 15 $\times$ 10^6 m^3 s^{-1}, so that for sediment loads in the range 10–40%, the minimum duration was two to nine weeks. In a similar analysis for the Mangala Valles system, Ghatan *et al.* (2005) estimated that 13 000–20 000 km^3 of material was removed by a flow rate averaging 5 $\times$ 10^6 m^3 s^{-1}, implying a flow duration of at least one to three months. A somewhat larger discharge of 1 $\times$ 10^7 m^3 s^{-1} was estimated for Mangala Valles by Leask *et al.* (2007), implying that the 13 000–20 000 km^3 of material was removed in about one month at a 40% sediment load and up to three months at a 20% load.

The use of sediment loads, in percentages of multiples of ten, to estimate flood durations requires further consideration. As noted in a detailed analysis by Kleinhans (2005), a water flood eroding its bed cannot change smoothly from having a low concentration of washload (i.e. essentially fully suspended) solids to being hyperconcentrated; two stable washload solid concentrations are allowed for a given flow speed and depth, but the load cannot change smoothly from the one to the other by bed erosion alone unless the flow speed passes a very large value. These results, summarised by Kleinhans (2005, his Figure 16.12), imply that, for the typical flow conditions deduced above, Martian floods could not carry more than about 2% solids by volume as washload, very much less than the values up to 40% by volume assumed by many workers. A flow could only be hyperconcentrated if it were discharged from its source in a hyperconcentrated state or had a large sediment load injected into it, say by a massive collapse of the channel wall. Hyperconcentrated discharge from the source would require extraction of the water from an aquifer under conditions that damaged the structural fabric of the aquifer and elutriated large amounts of fine solids. It is hard to assess the plausibility of such a process but it might explain the apparently very large aquifer permeabilities implied by the larger estimates of discharges on Mars (Table 16.1). Injection of a sudden load by channel-wall collapse is plausible but would inevitably be a very transient event compared with the duration of channel formation. In the next section a critical issue for Mars is quantified; the low-temperature physical conditions eventually force part of the solids load (in this case the ice crystals) to increase monotonically with time and distance from the source. It is therefore possible that, although a smooth transition cannot occur in Martian channels by bed erosion alone, it may occur through ice-crystal growth. However, because ice crystals and silicate clasts would be competing in their contribution to the washload, this process would presumably reduce the amount of silicates capable of being fully suspended in the flow. Thus this process does not help the flow to carry a greater washload of eroded silicates from the bed, and has no bearing on the issue of the time taken to erode a given depth of channel. This conclusion is equally true of hyperconcentrated flows caused by an initial high solids content in the released water or by channel-wall collapse; if anything, these processes imply a reduced ability to carry material eroded from the bed in suspension. Thus it appears that the critical issue is the volume fraction of eroded clasts that could be carried as bedload or suspended solids. Kleinhans (2005) discusses the large uncertainties in the factors governing bed erosion rate and sediment transport as bed and suspended load, and his arguments suggest that it is unlikely that the combination of all three transport mechanisms would lead to a total volume fraction of sediment greater than about 5%. Adopting this value would increase the flood durations mentioned above by a factor of four.

Durations of at least weeks to months are very much greater than the time scales of at most hours on which aquifer flow rates are predicted to decrease significantly if aquifer permeabilities have values comparable to those on Earth (Manga, 2004). If Martian permeability values are indeed similar to those of Earth, so that initially high water release rates declined dramatically, or if the load-carrying capacities of floods were much less than the tens of percentage points commonly assumed, then discharges would have to have continued for even longer periods of time at smaller volume fluxes and hence lower flow speeds (Kleinhans, 2005). However, lower flow speeds would mean that a given batch of water in the system would have

been exposed to Martian environmental conditions for a greater period of time while travelling a given distance, and this has a bearing on the maximum distance for which water can survive as a liquid on Mars, which is discussed below.

16.6 Water flow thermodynamics and rheology

The dynamics issues discussed in the previous section are clearly the major factors relevant to water flow in the proximal parts of outflow channels on Mars. However, two additional factors become progressively more important with distance from the source. These factors are both dictated by the environmental conditions of low ambient temperature and low atmospheric pressure. The low pressure can cause rapid rates of evaporation of water immediately after its release, enhancing initial cooling rates, but ultimately it is the low ambient temperature that dictates the final fate of the water, both via heat loss from the surface and through incorporation of the extremely cold surface materials at the base of the flow. The addition of the sediment load coupled with ice formation in the water eventually causes the rheology of the fluid to become non-Newtonian, with various implications for the water behaviour in distal parts of channels.

16.6.1 Water evaporation and consequent heat loss

Over much of the surface of Mars, the atmospheric pressure is low enough that water will boil spontaneously on being exposed to it, even if the water temperature is close to the freezing point (see Figure 16.2). The evaporation rate is proportional to the amount by which the vapour pressure of the water exceeds the local atmospheric pressure, and because the vapour pressure increases nearly exponentially with temperature, the evaporation rate is a very strong function of the water temperature. The latent heat of evaporation is extracted from the residual water and causes cooling. The cooling decreases the water vapour pressure and so the rate of cooling decreases as the temperature decreases. In low-lying areas on Mars the atmospheric pressure is high enough that water released at low to moderate temperatures will not boil, and even water that is hot enough to boil will cease to do so after it has cooled somewhat. Once boiling ceases, vapour loss by diffusion into the atmosphere still occurs, especially under windy conditions, but the mass loss rate and consequent heat loss rate are reduced greatly. Thus the detailed cooling history is strongly dependent on both the temperature of the water and the elevation relative to Mars datum of its release point.

As an example of the history of a flow strongly influenced by these issues, consider a source at an elevation where the surface atmospheric pressure is 610 Pa, just marginally less than the vapour pressure of water at the triple point, 610.5 Pa. Under these circumstances, water will continue to evaporate at a significant rate at all temperatures above the freezing point. Assume the water has a temperature of 30 °C and forms a flow with a depth of 50 m, then on a slope of $\tan^{-1}0.0007$ it flows away from its source at a speed of 5.5 m s^{-1} (see Figure 16.4). The initial vapour pressure of the water, P_v, is 4.23 kPa and so the difference between the water vapour pressure and the atmospheric pressure, P_a, is 3.62 kPa. The mass loss rate from the surface, dm/dt, is given by

$$dm/dt = z(P_v - P_a)[(M_w/2\pi G T_w)]^{1/2} \quad (16.19)$$

(Kennard, 1938), where M_w is the molecular weight of water, G is the universal gas constant, T_w is the absolute water temperature and z is the coefficient of evaporation. The empirically determined value of z is 0.94 (Tschudin, 1946). Therefore dm/dt is equal to 3.63 kg s^{-1} m^{-2}; the corresponding heat loss rate, the product of the mass loss rate and the latent heat of vaporisation, 1.78 MJ kg^{-1} at this temperature, is 6.46 MJ s^{-1} m^{-2}. Thus the initial values of the rates of decrease of depth and temperature of the water are 3.63 mm s^{-1} and 0.011 K s^{-1}, respectively. If these rates continued unchanged, the water would all have evaporated after 3.8 hours having travelled 76 km, and would have started to freeze after 45 minutes having travelled 15 km. In practice, the rates of change of depth and temperature both become smaller as the water vapour pressure decreases with the decreasing temperature, and the relevant equations describing these processes must be integrated numerically to follow the flow development. For this particular set of initial conditions, Figure 16.8a shows how depth and temperature evolve until the water freezing point is reached, and how the depth subsequently changes as evaporation continues at a constant temperature of 0 °C, so that progressive freezing of the water is taking place. The figure shows the changing water depth until the ice volume fraction in the water reaches 40%, at which point the presence of the ice crystals must have a significant effect on the rheology of the mixture, discussed in later sections. Figure 16.8b shows the equivalent information for water released at the same temperature, 30 °C, but in a flood initially 100 m deep, so that the initial flow speed is 8.7 m s^{-1} (see Figure 16.4). The illustrations in Figure 16.8 serve to underline how rapidly temperature and depth will change in the proximal part of a flood, and how long it will take for accumulation of ice crystals to significantly influence the water motion. These results, and analogous simulations for other water release temperatures and source elevations, would be directly applicable to Martian floods if the floods did not erode the surfaces over which they flowed. However, the observational evidence (see Burr *et al.*, this volume Chapter 10) suggests that erosion of cryosphere materials from channel beds, at least in the proximal parts of outflow channels, was a major factor in their development. This process is considered below.

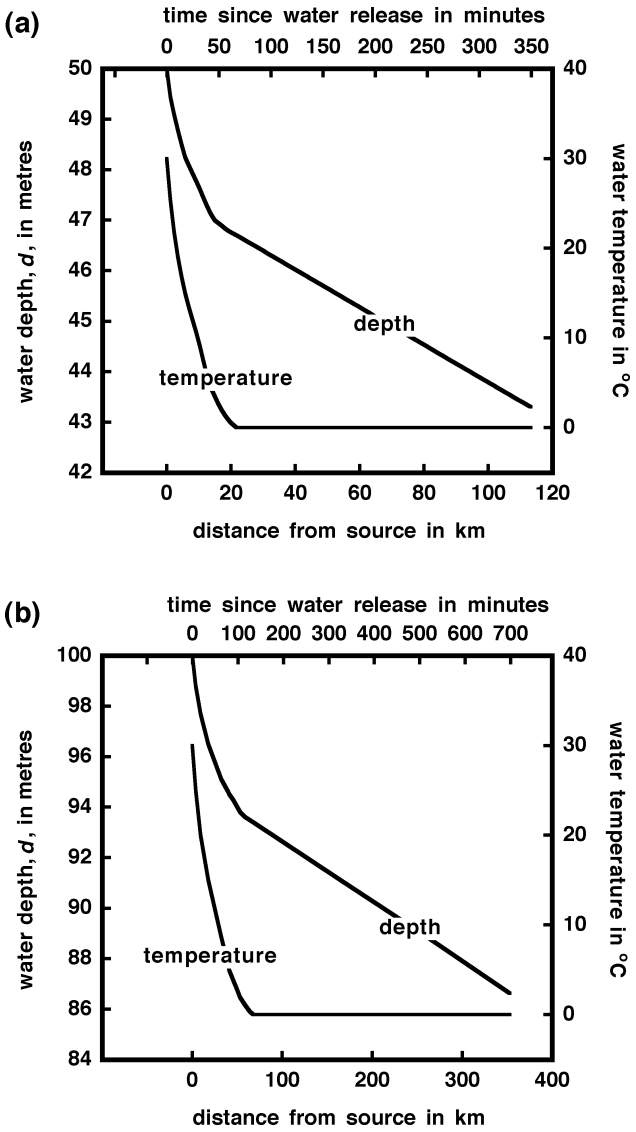

Figure 16.8. Variation of water depth and mean water temperature with distance from water release point in a channel on Mars. The time for which a given batch of water has been travelling is derived from the distance and the changing flow speed. The initial water temperature is taken as 30 °C. The elevation of the release point is such that the local atmospheric pressure is 610 Pa. In part (a) the initial water depth and speed are 50 m and 5.54 m s^{-1}, respectively; in part (b) they are 100 m and 8.69 m s^{-1}, respectively.

16.6.2 Thermal consequences of cryosphere erosion

The low Martian ambient temperature means that erosion of the surface involves not only the addition of a cold silicate sediment load to the water but also the addition of cryosphere ice. Transfer of sensible heat to both components, and of the latent heat needed to melt the ice, are both significant sources of water cooling, especially near channel sources where erosion rates are greatest. The calculations underlying Figure 16.8 imply that a source of proximal cooling in addition to evaporation will decrease the early-stage water evaporation rate. Thus, although the rate at which the temperature falls will increase, the rate at which the depth decreases will be reduced, relative to what is shown in the figure. When the water temperature reaches the freezing point, entrained cryosphere ice will no longer be melted, and the released floodwater will begin to freeze. The amount of freezing that takes place will be proportional to the volume fraction of cryosphere material entrained, and the total solid load carried by the water will be a mixture of eroded bedrock clasts, ice crystals derived from the cryosphere, and ice crystals produced by freezing of the original water. It is the total solid load volume fraction that will influence the bulk rheology of the fluid.

Consideration of the detailed consequences of eroding the cryosphere (Bargery, 2007) shows that the minimum water volumes found in the past by assuming that the water has a maximum sediment-carrying capacity are probably underestimates. To illustrate this, ignore the initial rapid cooling of the water and consider the addition of cryosphere materials after the water has cooled to its freezing temperature, T_f (∼273.15 K). Consider a volume V_w of this water, a fraction ϕ of which freezes due to entrainment of a volume V_c of cryosphere, of which ice occupies a volume fraction q. The heat required to warm the cryosphere materials from the ambient temperature T_a (∼210 K) to the water temperature T_f is $(T_f - T_a)V_c[q\rho_i c_i + (1-q)\rho_r c_r]$ where ρ_i and ρ_r are the densities of ice and rock, taken as 917 and 3000 kg m^{-3}, respectively, at cryosphere temperatures and c_i and c_r are the corresponding specific heats at constant pressure, 1900 and 700 J kg^{-1} K^{-1}. The heat released by partial freezing of the water is $\phi V_w \rho_w L_i$ where ρ_w is the water density, ∼1000 kg m^{-3}, and L_i is the latent heat of fusion of ice, ∼3.35 × 10^5 J kg^{-1}. Equating the two results in

$$\begin{aligned} V_w/V_c &= \{(T_f - T_a)[q\rho_i c_i + (1-q)\rho_r c_r]\}/[\phi\rho_w L_i] \\ &= K'/\phi, \end{aligned} \tag{16.20}$$

where K' is a constant. Inserting the relevant material properties specified earlier and using a value of $q = 0.15$, suggested by the cryosphere models of Hanna and Phillips (2005), produces $K' = 0.38\,575$. The water that freezes changes its volume because of the differing densities of water and ice and so the volume fraction of solids in the mixture after incorporation of cryosphere material and partial water freezing is s where

$$s = \frac{[1 + \phi(V_w/V_c)(\rho_w/\rho_i)]}{[1 + (1-\phi)(V_w/V_c) + \phi(V_w/V_c)(\rho_w/\rho_i)]}. \tag{16.21}$$

Substituting for (V_w/V_c) and solving this equation for ϕ:

$$\phi = sK'\rho_i/(sK'\rho_i + \rho_i - s\rho_i - sK'\rho_w + K'\rho_w). \tag{16.22}$$

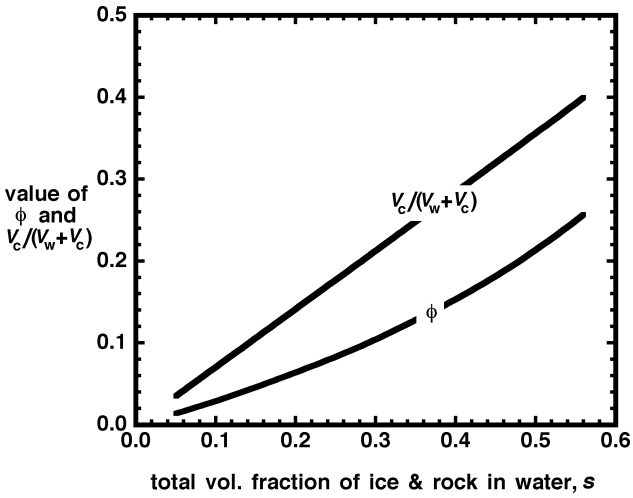

Figure 16.9. For water entraining eroded cryosphere material, the curves show the changes in the volume fraction of the original water that has frozen, ϕ, and the fraction of the total fluid volume that is cryosphere material, $[V_c/(V_w + V_c)]$, as a function of the total volume fraction of solids (ice and rock) in the water, s.

Figure 16.9 shows how s is related to $[V_c/(V_w + V_c)]$, the fraction of the total fluid volume that is cryosphere material. Consider the traditional assumption that the maximum sediment load that can be carried by a water flood is at least $[V_c/(V_w + V_c)] = 0.3$, i.e. 30% solids by volume. Ignoring the matter of cryosphere incorporation causing partial water freezing would have led to the conclusion that the volume of water passing through the channel was $(V_w/V_c) = 2.333$ times the missing volume eroded from the channel. However, when account is taken of the water freezing issue it is seen that if the true final volume fraction of rock *and ice* in the flowing fluid is $s = 0.3$, the true volume of water passing through the channel is $(V_w/V_c) = 3.701$ times the eroded volume, nearly 59% more water than the simple analysis would have predicted. If the upper limit for sediment transport is taken as 40% by volume, the traditional method would have implied $(V_w/V_c) = 1.500$ times the missing volume eroded from the channel, whereas using $s = 0.4$ implies $(V_w/V_c) = 2.517$ times the eroded volume, about 68% more water.

To illustrate the importance of the results presented immediately above, consider Figure 16.8a. The parameters used to generate this figure (an initial water depth of 50 m, a flow speed of 20 m s^{-1}, and a release location where the atmospheric pressure is close to the vapour pressure of water at the triple point) are similar to those relevant to the Mangala Valles channel system (Leask *et al.*, 2007). This channel shows strong indications of floor scouring for 150 km from its source (Burr *et al.*, this volume Chapter 10) and displays some erosional features for at least a further 100 km (Neather and Wilson, 2007). Thus, it seems likely that erosion continued in the case of this channel for, say, 250 km from the source. At this distance, Figure 16.8a implies that 25% of the water would already have been frozen due to evaporation alone. If 250 km from the source is identified as the distance at which the changing rheology causes a drastic change in erosive power and 40% total solids is adopted as the critical load that leads to that change in behaviour, a further 15% by volume of solids, a mixture of ice and rock, should have been added to the water. This corresponds to setting $s = 0.15$, for which $(V_w/V_c) = 8.4$; thus, in this case it may be concluded that the volume of water that must have passed through the channel to produce the observed features was not 2.5 times the eroded volume but instead more than 8 times that volume. These simple illustrations are imperfect in that they do not treat the two main sources of heat loss from Martian flood waters simultaneously; however, they serve to make it clear how important it is that a comprehensive model of conditions in outflow channels on Mars should be developed.

16.6.3 Influence of ice formation and sediment load on rheology

It was asserted above that the loading of water in an outflow channel by 30–40 volume per cent solids will change its rheology. The first-order effect is likely to be the generation of a yield strength causing an evolution from Newtonian to non-Newtonian behaviour. If the fluid behaves like the simplest non-Newtonian material, a Bingham plastic, the presence of a yield strength in turbulent flow (Malin, 1998) is likely to result in the formation of pods of fluid within which there is little deformation, shear being concentrated in the regions between these pods. The sizes of these pods will be a large fraction of the depth of the flow. The lack of deformation within the pods will encourage segregation of the solids from the liquid driven by buoyancy forces, silicates tending to sink and ice crystals tending to rise. However, the random tumbling of the pods in the turbulent flow will mean that no significant net segregation will occur.

The bulk density, β, yield strength, τ_y, and plastic viscosity, η, of the bulk fluid control two dimensionless groups, the Reynolds number (equal to $4Ru\beta/\eta$) and the Hedstrom number (a dimensionless resistance to shear, defined as $16R^2\tau_y\beta^2/\eta^2$), that characterise the internal fluid motion. When the sediment/ice load and hence the yield strength become large enough, the Hedstrom number will reach a critical value, itself a function of the Reynolds number, that causes a progressive transition towards laminar flow. If completely laminar conditions are reached, the fluid will develop plug flow, with an unsheared raft of fluid extending down from the surface and moving over a sheared zone beneath, extending down to the bed. The stresses exerted by the laminar sheared zone on the bed will

be much smaller than those involved in turbulent flow, and so bed erosion should decrease dramatically or cease completely. If these conditions are approached, the unsheared material will no longer be tumbling, and gravitational sinking of the silicate clasts and flotation of ice crystals can begin. In this way a semi-continuous ice raft may begin to form on the flow surface. However, a rapid transition to complete elimination of turbulence is not expected, because if extensive segregation of the solids occurred, the resulting Newtonian water would immediately become turbulent again, and begin once more to erode and entrain bed material. Thus it should be expected that feedback loops cause conditions in the fluid to hover close to the critical Hedstrom number for as long as possible (Bargery and Wilson, 2006).

If ice raft formation does begin, there will not be a continuous raft, at least not initially; collisions with the banks and deformation wherever the bed slope changes will cause breaks in the coverage, and in these places water at 0 °C will be exposed to the atmosphere and will continue to evaporate and cool. However, on the undisturbed parts of the raft surface the temperature will decrease to the ambient, ∼210 K, and at this temperature any mass and heat loss by evaporation will be essentially negligible. Thus, apart from a small amount of cooling through cracks in the ice (which may become smaller in number as the ice thickness increases downstream), significant heat loss from the upper surface of the flood will cease and only heat loss to the underlying cryosphere will be important. Furthermore, the cessation, or at least reduction, of turbulence and consequent settling of silicates is likely to cause a progressive change from bed erosion to deposition of a growing layer of solids at 0 °C on the bed. As a result, conduction from the body of the flow into the ground will also be minimised. This potential influence of the presence of ice crystals as well as suspended solids on the balance between bed erosion and sediment deposition may cause a systematic difference between the downstream variation of bedforms produced by major water floods on Earth and Mars. Although erosion of the bed may not occur where ice rafts are present, impacts of the ice rafts with the topography confining the flow will cause some erosion. Such erosion of the channel banks is observed in cold-climate (but non-glacial) rivers on Earth (e.g. Martini *et al.*, 1993).

Another geomorphic indicator of the presence of ice, which is commonly observed in terrestrial glacial settings, is kettle holes. Kettle holes are depressions that result from the stranding of large ice blocks (maximum size order tens of metres in diameter) during glacial meltwater flow (e.g. Maizels, 1977; Russell, 1993; Tómasson, 1996). In the largest contemporary floods, which occur from beneath glaciers (Björnsson, this volume Chapter 4), these blocks

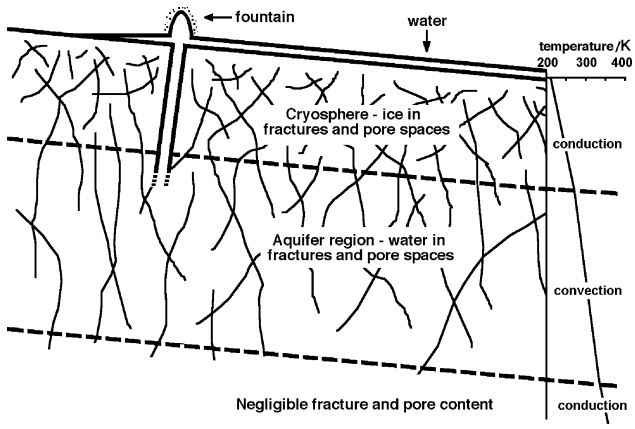

Figure 16.10. Diagram showing the key structures and processes involved in the release of water onto the surface of Mars from confined aquifers.

are commonly produced by breakage and collapse of the glacier margin during sub-, en-, or proglacial flooding (e.g. Sugden *et al.*, 1985). Subsequent melting of the ice blocks most commonly produces simple depressions, but these depressions may have rims or even contain mounds, depending on the amount of sediment carried by the block and its degree of burial (Maizels, 1992). Kettle holes have been inferred in two outflow channels on Mars, for a population of simple depressions in Maja Valles (Chapman *et al.*, 2003) and for a population of raised-rim depressions in Athabasca Valles (Gaidos and Marion, 2003), although the Athabasca Valles population has been hypothesised to have other origins (Burr *et al.*, this volume Chapter 10).

16.7 Closing summary

While the basic processes occurring in outflow channels on Mars and on Earth are likely to have been the same, there are numerous differences of detail imposed by the Martian environment (Figure 16.10). For much of the planet's history, major water reservoirs on Mars were probably located at depths of several kilometres below the surface, being released by tectonic and volcanic (and possibly impact) events that disrupted the cryosphere. Thus, despite the low surface temperature, quite a wide range of released water temperatures was possible. Exposure to the low-pressure atmosphere would have caused vigorous evaporation of warm water and rapid cooling; cooling would have been enhanced by the erosion and incorporation of rock and ice from the cryosphere. For a given water depth, water flow speeds on Mars would have been less than on Earth by the square root of the ratio of the respective accelerations due to gravity. This only represents a difference by a factor of 1.6, and so bed erosion processes, and the consequent evolution from supercritical to subcritical flow conditions, would probably have been similar. However, we have no

direct observations of the formation of outflow channels by floods on the scale of the Martian outflows, the most recent on Earth being the prehistoric Missoula Flood. Thus, there are still uncertainties about the relative importance of various bed erosion processes, especially cavitation.

The importance of ice formation in Martian water floods cannot be overemphasized. On Earth, evolution of the rheology of flowing water is dictated by incorporation and transport of sediments, and changes in topographically driven flow speed control changes in erosion and deposition. On Mars, the rheological influence of increasing amounts of ice crystals must also be considered. A full understanding of water flow in Martian outflow channels awaits a comprehensive model incorporating all of the issues discussed in this review.

Even if all of the basic physics has been identified, there are still numerous uncertainties in the parameters required for such models. For example, the only *in situ* grain size determinations in what may be fluvial deposits on Mars are those from the Viking 1, Viking 2 and Pathfinder lander sites (Golombek and Rapp, 1997; Golombek *et al.*, 2003); however, camera resolution limitations mean that we have no reliable information on the sub-centimetre size fractions, which have a very great influence on flow conditions (Kleinhans, 2005). This problem could be remedied by suitably targeted next-generation landers with higher-resolution optics. The other most important uncertainties are in the physical properties of aquifers (permeability, porosity and mean water temperature) and of the cryosphere (permeability, porosity and ice content). Although some information on subsurface structure may be gleaned from orbiting RADAR systems (e.g. MARSIS on Mars Express – Picardi *et al.*, 2005), it is hard to see how major improvements can be made without ground-penetrating radar, active seismic experiments and, preferably, drilling from surface landers or penetrators.

Notation

Symbol	Definition	Units
D	depth of tops of aquifer, 5−8	km
D_{50}	clast size such that 50% of clasts are smaller than D_{50}, ∼0.1	m
D_{84}	clast size such that 84% of clasts are smaller than D_{50}, ∼0.48	m
D_{90}	clast size such that 90% of clasts are smaller than D_{50}, ∼0.6	m
F	volume flux of water flowing through channel	$m^3\ s^{-1}$
Fr	Froude number for flow in channel	
G	universal gas constant, 8314	$J\,kmol^{-1}\,K^{-1}$
H	vertical extents of aquifer, ∼6	km
K	bulk thermal conductivity of an aquifer, ∼2.5	$W\,m^{-1}\,K^{-1}$
K'	constant appearing in Eq. (16.19), ∼0.38575	
L_i	latent heat of fusion of ice, $\sim 3.35 \times 10^5$	$J\,kg^{-1}$
M_w	molecular weight of water, 18.02	$kg\,kmol^{-1}$
P_a	atmospheric pressure, ∼600	Pa
P_v	saturation vapour pressure of water	Pa
Q	volume fraction of solids in water–solids mixture	
R	hydraulic radius of the channel	m
S	sine of channel bed slope	
T_a	ambient temperature of shallow cryosphere, ∼210	K
T_c	mean temperature of cryosphere, ∼240	K
T_f	melting temperature of ice ∼273.15	K
T_r	average temperature in water rising in fractures, ∼300	K
T_w	mean water temperature in surface flow	K
U	rise speed of water in crustal fracture, ∼40−50	$m\,s^{-1}$
V_c	volume of cryosphere material entrained by water	m^3
V_s	volume of cryosphere material eroded from channel	m^3
V_w	volume of water in water–solids mixture	m^3
W	width of crustal fracture, ∼2	m
Z	topographic height difference	km
c_i	specific heat at constant pressure of cryosphere ice, ∼1900	$J\,kg^{-1}\,K^{-1}$
c_r	specific heat at constant pressure of cryosphere silicate rock, ∼700	$J\,kg^{-1}\,K^{-1}$
c_w	specific heat at constant pressure of water, 4175	$J\,kg^{-1}\,K^{-1}$
d	depth of water in channel	m
dm/dt	mass flux per unit area of evaporating water molecules	$kg\,s^{-1}\,m^{-2}$
dP/dz	pressure gradient driving water up fracture, ∼950	$Pa\,m^{-1}$
dT/dx	temperature gradient controlling heat flow away from fracture	$K\,m^{-1}$

dT/dz	vertical temperature gradient across aquifer	$K\,m^{-1}$
f	friction factor for motion of water against wall of fracture, $\sim 10^{-2}$	
f_c	friction factor for motion of water in channel	
g	acceleration due to gravity on Mars, ~ 3.72	$m\,s^{-2}$
k	permeability of aquifer	
k_c	critical permeability of aquifer	
n	Manning coefficient for water flow in channel	$s\,m^{-1/3}$
q	volume fraction of ice in cryosphere, ~ 0.15	
r	typical size of bed roughness elements, $\sim D_{50}$	m
s	volume fraction of all solids in water–solid mixture in channel	
w	width of channel	m
z	empirical coefficient of evaporation efficiency, 0.94	
ΔT_a	adiabatic temperature change in water rising in fractures	K
ΔT_c	average decrease in temperature of water rising in fracture, ~ 0.5	K
Φ	factor by which flow speed must increase for cavitation, ~ 2	
α	slope of channel bed	radian
α_w	volume thermal expansion coefficient of water, $(2.5-5) \times 10^{-4}$	K^{-1}
β	bulk density of water–solid mixture in channel	$kg\,m^{-3}$
δT	decrease in temperature of water rising in fracture	K
η	plastic viscosity of water–solid mixture in channel	Pa s
κ	thermal diffusivity of cryosphere material, $\sim 7 \times 10^{-7}$	$m^2\,s^{-1}$
λ	depth to which heat penetrates into fracture wall from water	m
μ_w	viscosity of water	Pa s
ρ_i	density of ice, ~ 917	$kg\,m^{-3}$
ρ_r	density of silicate rock, ~ 3000	$kg\,m^{-3}$
ρ_w	density of water, ~ 1000	$kg\,m^{-3}$
σ_g	geometric standard deviation of the bed clast size distribution, ~ 2.9	
τ	transit time of water rising through fracture, $\sim 60-100$	s
τ_y	yield strength of water–solid mixture in channel	Pa
ϕ	fraction of water that freezes due to entrainment of cryosphere	

Acknowledgements

We are grateful to Maarten Kleinhans and Michael Manga for thoughtful and constructive comments on this chapter.

References

Andrews-Hanna, J. C. and Phillips, R. J. (2007). Hydrological modeling of outflow channels and chaos regions on Mars. *Journal of Geophysical Research*, **112** (E08001), doi:10.1029/2006JE002881.

ASCE (1963). Friction factors in open channels (Task force report). *Journal of the Hydraulics Division, Proceedings of the American Society of Civil Engineers*, **89** (HY2), 97–143.

Baker, V. R. (1979). Martian channel morphology: Maja and Kasei Valles. *Journal of Geophysical Research*, **84** (B14), 7,961–7,983.

Baker, V. R. (1982). *The Channels of Mars*. Austin, TX: University of Texas Press.

Baker, V. R. (2001). Water and the Martian landscape. *Nature*, **412**, 228–236.

Bargery, A. S. (2007). Aqueous eruption and channel flow on Mars during the Amazonian epoch. Unpublished Ph.D. thesis, Lancaster University, UK.

Bargery, A. S. and Wilson, L. (2006). Modelling water flow with bedload on the surface of Mars. In *Lunar and Planetary Science Conference XXXVI*, Abstract 1218. Houston, TX: Lunar and Planetary Institute.

Bargery, A. S., Wilson, L. and Mitchell, K. L. (2005). Modelling catastrophic floods on the surface of Mars. In *Lunar and Planetary Science Conference XXXV*, Abstract 1961. Houston, TX: Lunar and Planetary Institute.

Bargery, A. S. and Wilson, L. (Submitted). Dynamics of the ascend and eruption of water containing dissolved CO_2 on Mars. *Journal of Geophysical Research*, 2009 JE003403.

Barnes, H. L. (1956). Cavitation as a geological agent. *American Journal of Science*, **254**, 493–505.

Bathurst, J. C. (1993). Flow resistance through the channel network. In *Channel Network Hydrology*, eds. K. Beven and M. J. Kirkby. Chichester, UK: Wiley, pp. 69–98.

Burr, D. M., McEwen, A. S. and Sakimoto, S. E. H. (2002a). Recent aqueous floods from the Cerberus Fossae. *Geophysical Research Letters*, **29** (1), doi:10.1029/2001GL013345.

Burr, D. M., Grier, J. A., McEwen, A. S. and Keszthelyi, L. P. (2002b). Repeated aqueous flooding from the Cerberus Fossae: evidence for very recently extant, deep groundwater on Mars. *Icarus*, **155**, 53–73.

Burr, D. M., Carling, P. A., Beyer, R. A. and Lancaster, N. (2004). Flood-formed dunes in Athabasca Valles, Mars:

morphology, modeling, and implications. *Icarus*, **171**, 68–83.

Burt, D. M. and Knauth, L. P. (2003). Electrically conducting, Ca-rich brines, rather than water, expected in the Martian subsurface. *Journal of Geophysical Research*, **108** (E4), 8026, doi:10.1029/2002JE001862.

Carling, P. A. (1996). Morphology, sedimentology and palaeohydraulic significance of large gravel dunes, Altai Mountains, Siberia. *Sedimentology*, **43**, 647–664.

Carr, M. H. (1979). Formation of Martian flood features by release of water from confined aquifers. *Journal of Geophysical Research*, **84** (B6), 2,995–3,007.

Carr, M. H. (2002). Elevations of water-worn features on Mars: implications for circulation of groundwater. *Journal of Geophysical Research*, **107** (E12), 5131, doi:10.1029/2002JE001845.

Carr, M. H. and Clow, G. D. (1981). Martian channels and valleys: their characteristics, distribution, and age. *Icarus*, **48**, 250–253.

Chadwick Jr., W. W. and Embley, R. W. (1998). Graben formation associated with recent dike intrusions and volcanic eruptions on the mid-ocean ridge. *Journal of Geophysical Research*, **103** (B5), 9807–9825, doi:10.1029/1997JB02485.

Chapman, M. G., Hare, T. M., Russell, A. J. and Gudmundsson, M. T. (2003). Possible Juventae Chasma subice volcanic eruptions and Maja Valles ice outburst floods on Mars: implications of Mars Global Surveyor crater densities, geomorphology, and topography. *Journal of Geophysical Research*, **108** (E10), 5113, doi:10.1029/2002JE002009.

Clifford, S. M. (1987). Polar based melting on Mars. *Journal of Geophysical Research*, **92** (B9), 9,135–9,152.

Clifford, S. M. (1993). A model for the hydrologic and climatic behaviour of water on Mars. *Journal of Geophysical Research*, **98** (E6), 10,973–11,016.

Clifford, S. M. and Parker, T. J. (2001). The evolution of the Martian hydrosphere: implications for the fate of a primordial ocean and the current state of the northern plains. *Icarus*, **154**, 40–79, doi:10.1006/icar.2001.6671.

Coleman, N. M. (2003). Aqueous flows carved the outflow channels on Mars. *Journal of Geophysical Research*, **108** (E5), 5039, doi:10.1029/2002JE001940.

Coleman, N. M. (2004). Ravi Vallis, Mars-paleoflood origin and genesis of secondary chaos zones. In *Lunar and Planetary Science Conference XXXV*, Abstract 1299. Houston, TX: Lunar and Planetary Institute.

Coleman, N. M. (2005). Martian megaflood triggered chaos formation, revealing groundwater depth, cryosphere thickness, and crustal heat flux. *Journal of Geophysical Research*, **110** (E12S20), doi:10.1029/2005JE002419.

De Hon, R. A. and Pani, E. A. (1993). Duration and rates of discharge: Maja Valles, Mars. *Journal of Geophysical Research*, **98** (E5), 9,128–9,138.

Diamond, L. W. and Akinfiev, N. N. (2003). Solubility of CO_2 in water from –1.5 to 100 °C and from 0.1 to 100 MPa: evaluation of literature data and thermodynamic modelling. *Fluid Phase Equilibria*, **208**, 265–290, doi:10.1016/S0378–3812(03)00041–4.

Dixon, J. E. (1997). Degassing of alkalic basalts. *American Mineralogist*, **82**, 368–378.

Dohm, J. M. *et al.* (2001a). Ancient drainage basin of the Tharsis Region, Mars: potential source for outflow channel systems and putative oceans or paleolakes. *Journal of Geophysical Research*, **106** (E12), 32,943–32,958.

Dohm, J. M. *et al.* (2001b). Latent outflow activity for Western Tharsis, Mars: significant flood record exposed. *Journal of Geophysical Research*, **106** (E6), 12,301–12,314.

Edlund, S. J. and Heldmann, J. L. (2006). Correlation of subsurface ice content and gulley locations on Mars: testing the shallow aquifer theory of gulley formation. In *Lunar and Planetary Science Conference XXXVII*, Abstract 2049. Houston, TX: Lunar and Planetary Institute.

Gaidos, E. and Marion, G. (2003). Geological and geochemical legacy of a cold early Mars. *Journal of Geophysical Research*, **108** (E6), 5055, doi:10.1029/2002JE002000.

Gay, E. C., Nelson, P. A. and Armstrong, W. P. (1969). Flow properties of suspensions with high solids concentrations. *Journal of the American Institute of Chemical Engineers*, **15**, 815–822.

Gerlach, T. M. (1986). Exsolution of H_2O, CO_2, and S during eruptive episodes at Kilauea volcano, Hawaii. *Journal of Geophysical Research*, **91** (B12), 12,177–12,185.

Ghatan, G. J., Head, J. W. and Wilson, L. (2005). Mangala Valles, Mars: assessment of early stages of flooding and downstream flood evolution. *Earth, Moon and Planets*, **96** (1–2), 1–57, doi:10.1007/s11038–005-9009-y.

Gioia, G. and Bombardelli, F. A. (2002). Scaling and similarity in rough channel flows. *Physical Review Letters*, **88** (1), doi:10.1103/PhysRevLett.88.014501.

Golombek, M. P. and Rapp, D. (1997). Size-frequency distributions of rocks on Mars and Earth analog sites: implications for future landed missions. *Journal of Geophysical Research*, **102** (E2), 4117–4129.

Golombek, M. P., Cook, R. A., Moore, H. J. and Parker, T. J. (1997). Selection of the Mars Pathfinder landing site. *Journal of Geophysical Research*, **102** (E2), 3967–3988, doi:10.1029/96JE03318.

Golombek, M. P., Haldemann, A. F. C., Forsberg-Taylor, N. K. *et al.* (2003). Rock size-frequency distributions on Mars and implications for Mars Exploration Rover landing safety and operations. *Journal of Geophysical Research*, **108** (E12), 8086, doi:10.1029/2002JE002035.

Grant, G. E. (1997). Critical flow constrains flow hydraulics in mobile-bed streams: a new hypothesis. *Water Resources Research*, **33** (2), 349–358.

Gulick, V. C. (1998). Magmatic intrusions and a hydrothermal origin for fluvial valleys on Mars. *Journal of Geophysical Research*, **103** (E8), 19,365–19,387.

Gulick, V. C. (2001). Origin of the valley networks on Mars: a hydrological perspective. *Geomorphology*, **37**, 241–268.

Hanna, J. C. and Phillips, R. J. (2005). Hydrological modeling of the Martian crust with application to the pressurization of

aquifers. *Journal of Geophysical Research*, **110**, E01004, doi:10.1029/2004JE002330.

Hanna, J. C. and Phillips, R. J. (2006). Tectonic pressurization of aquifers in the formation of Mangala and Athabasca Valles, Mars. *Journal of Geophysical Research*, **111**, E03003, doi:10.1029/2005JE002546.

Harris, D. M. (1981). The concentration of CO_2 in submarine tholeiitic basalts. *Journal of Geology*, **89**, 689–701.

Head, J. W., Wilson, L. and Mitchell, K. L. (2003a). Generation of recent massive water floods at Cerberus Fossae, Mars by dike emplacement, cryospheric cracking, and confined aquifer groundwater release. *Geophysical Research Letters*, **30** (11), 1577, doi:10.1029/2003GL017135.

Head, J. W., Mustard, J. F., Kreslavsky, M. A., Milliken, R. E. and Marchant, D. R. (2003b). Recent ice ages on Mars. *Nature*, **426**, 797–802, doi:10.1038/nature02114.

Head, J. W., Marchant, D. R. and Ghatan, G. J. (2004). Glacial deposits on the rim of a Hesperian-Amazonian outflow channel source trough: Mangala Valles, Mars. *Geophysical Research Letters*, **31**, L10701, doi:10.1029/2004GL020294.

Heldmann, J. L. and Mellon, M. T. (2004). Observations of martian gullies and constraints on potential formation mechanisms. *Icarus*, **168**, 285–304.

Herschel, C. (1897). On the origin of the Chézy formula. *Journal of the Association of Engineering Societies*, **18**, 2–51.

Hjülstrom, F. (1932). Das transportvermögen der flüsse und die bestimmung des erosionsbetrages. *Geografiska Annaler*, **14**, 244–258.

Hoffman, N. (2000). White Mars: a new model for Mars' surface and atmosphere based on CO_2. *Icarus*, **146**, 326–342.

Hoffman, N. (2001). Explosive CO_2-driven source mechanisms for an energetic outflow "jet" at Aromatum Chaos, Mars. In *Lunar and Planetary Science Conference XXXII*, Abstract 1257. Houston, TX: Lunar and Planetary Institute.

Hunt, A. G., Grant, G. E. and Gupta, V. K. (2006). Spatio-temporal scaling of channels in braided streams. *Journal of Hydrology*, **322**, 192–198.

Kaye, G. W. C. and Laby, T. H. (1995). *Tables of Physical and Chemical Constants*, 16th edn. Harlow, Essex, UK: Longman.

Kennard, E. H. (1938). *Kinetic Theory of Gases*, 1st edn. New York, NY: McGraw-Hill.

Kleinhans, M. G. (2005). Flow discharge and sediment transport models for estimating a minimum timescale of hydrological activity and channel and delta formation on Mars. *Journal of Geophysical Research*, **110**, E12003, doi:10.1029/2005JE002521.

Knudsen, J. G. and Katz, D. L. (1958). *Fluid Dynamics and Heat Transfer*, New York, NY: McGraw-Hill.

Komar, P. D. (1979). Comparisons of the hydraulics of water flows in Martian outflow channels with flows of similar scale on Earth. *Icarus*, **37**, 156–181.

Komar, P. D. (1980). Modes of sediment transport in channelized water flows with ramifications to the erosion of the Martian outflow channels. *Icarus*, **42**, 317–329.

Komatsu, G. and Baker, V. R. (1997). Paleohydrology and flood geomorphology of Ares Vallis. *Journal of Geophysical Research*, **102** (E2), 4,151–4,160.

Komatsu, G., Ori, G. G., Ciarcelluti, P. and Litasov, Y. D. (2004). Interior layered deposits of Valles Marineris, Mars: analogous subice volcanism related to Baikal Rifting, Southern Siberia. *Planetary and Space Science*, **52**, 167–187.

Leask, H. J., Wilson, L. and Mitchell, K. L. (2004). The formation of Aromatum Chaos and the water discharge rate at Ravi Vallis. In *Lunar and Planetary Science Conference XXXV*, Abstract 1544. Houston, TX: Lunar and Planetary Institute.

Leask, H. J., Wilson, L. and Mitchell, K. L. (2006a). Formation of Ravi Vallis outflow channel, Mars: morphological development, water discharge, and duration estimates. *Journal of Geophysical Research*, **111**, E08070, doi:10.1029/2005JE002550.

Leask, H. J., Wilson, L. and Mitchell, K. L. (2006b). Formation of Mangala Fossa, the source of the Mangala Valles, Mars: morphological development as a result of volcano-cryosphere interactions. *Journal of Geophysical Research*, **112**, E02011, doi:10.1029/2005JE002644.

Leask, H. J., Wilson, L. and Mitchell, K. L. (2006c). Formation of Aromatum Chaos, Mars: morphological development as a result of volcano-ice interactions. *Journal of Geophysical Research*, **111**, E08071, doi:10.1029/2005JE002549.

Leask, H. J., Wilson, L. and Mitchell, K. L. (2007). Formation of Mangala Valles outflow channel, Mars: morphological development, and water discharge and duration estimates. *Journal of Geophysical Research*, **112**, E08003, doi:10.1029/2006JE002851.

Leverington, D. W. (2004). Volcanic rilles, streamlined islands, and the origin of outflow channels on Mars. *Journal of Geophysical Research*, **109**, E10011, doi:10.1029/2004JE002311.

Lognonne, P. (2005). Planetary seismology. *Annual Review of Earth and Planetary Sciences*, **33**, 571–604.

Maizels, J. K. (1977). Experiments on the origin of kettle-holes. *Journal of Glaciology*, **18** (79), 291–303.

Maizels, J. (1992). Boulder ring structures produced during jökulhlaup flows: origin and hydraulic significance. *Geografiska Annaler*, **A74** (1), 21–33.

Malin, M. R. (1998). Turbulent pipe flow of Herschel-Bulkley fluids. I*nternational Communications in Heat and Mass Transfer*, **25** (3), 321–330.

Manga, M. (2004). Martian floods at Cerberus Fossae can be produced by groundwater discharge. *Geophysical Research Letters*, **31**, L02702, doi:10.1029/ 2003GL018958.

Manning, R. (1891). On the flow of water in open channels and pipes. *Transactions of the Institute of Civil Engineers of Ireland*, **20**, 161–207.

Martini, I. P., Kwong, J. K. and Sadura, S. (1993). Sediment ice rafting and cold climate fluvial deposits: Albany River, Ontario, Canada. *Special Publications of the International Association for Sedimentology*, **17**, 63–76.

Masursky, H., Boyce, J. M., Dial, A. L., Schaber, G. G. and Strobel, M. E. (1977). Classification and time of formation of

Martian channels based on Viking data. *Journal of Geophysical Research*, **82** (28), 4,016–4,038.

McGovern, P. J., Solomon, S. C., Smith, D. E. *et al.* (2002). Localized gravity/topography admittance and correlation spectra on Mars: implications for regional and global evolution. *Journal of Geophysical Research*, **107** (E12), 5136, doi:10.1029/2002JE001854.

McKenzie, D. and Nimmo, F. (1999). The generation of Martian floods by the melting of ground ice above dykes. *Nature*, **397** (6716), 231–233, doi:10.1038/16649.

Mellon, M. T. and Phillips, R. J. (2001). Recent gullies on Mars and the source of liquid water. *Journal of Geophysical Research*, **106** (E10), 23,165–23,179.

Milton, D. J. (1974). Carbon dioxide hydrate and floods on Mars. *Science*, **183**, 654–656.

Neather, A. and Wilson, L. (2007). Morphological features and discharge estimates for the medial part of the Mangala Valles channel system, Mars. In *Lunar and Planetary Science Conference XXXIII*, Abstract 1265. Houston, TX: Lunar and Planetary Institute.

Neukum, G., Jaumann, R., Hoffmann, H. *et al.* and the HRSC Co-Investigator Team (2004). Recent and episodic volcanic and glacial activity on Mars revealed by the High Resolution Stereo Camera. *Nature*, **432**, 971–979, doi:10.1038/nature03231.

Neumann, G. A., Zuber, M. T., Wieczorek, M. A. *et al.* (2004). Crustal structure of Mars from gravity and topography. *Journal of Geophysical Research*, **109** (E8), 8002, doi:10.1029/2004JE002262.

Nimmo, F. and Tanaka, K. (2005). Early crustal evolution of Mars. *Annual Review of Earth and Planetary Sciences*, **33**, 133–161.

Ogawa, Y., Yamagishi, Y. and Kurita, K. (2003). Evaluation of melting process of the permafrost on Mars: its implication for surface features. *Journal of Geophysical Research*, **108** (E4), 8046, doi:10.1029/2002JE001886.

Oost-hoek, J. H. P., Zegers, T. E., Rossi, A., Foing, B., Neukum, G. and the HRSC Co-Investigator Team (2007). 3D mapping of Aram Chaos: a record of fracturing and fluid activity. In *Lunar and Planetary Science Conference XXXVIII*, Abstract 1577. Houston, TX: Lunar and Planetary Institute.

Ori, G. G. and Mosangini, C. (1998). Complex depositional systems in Hydraotes Chaos, Mars: an example of sedimentary process interactions in the Martian hydrological cycle. *Journal of Geophysical Research*, **103** (E10), 22,713–22,723.

Picardi, G. *et al.* (2005). Radar soundings of the subsurface of Mars. *Science*, **310** (5756), 1925–1928, doi:10.1126/science.1122165.

Rice, J. W., Christensen, P. R., Ruff, S. W. and Harris, J. C. (2003). Martian fluvial landforms: a THEMIS perspective after one year at Mars. In *Lunar and Planetary Science Conference XXXIV*, Abstract 2091. Houston, TX: Lunar and Planetary Institute.

Robinson, M. S. and Tanaka, K. L. (1990). Magnitude of a catastrophic flood event at Kasei Valles, Mars. *Geology*, **18**, 902–905.

Rossbacher, L. A. and Judson, S. (1981). Ground ice on Mars: inventory, distribution, and resulting landforms. *Icarus*, **45**, 39–59.

Rubin, A. M. (1992). Dike-induced faulting and graben subsidence in volcanic rift zones. *Journal of Geophysical Research*, **97** (B2), 1839–1858.

Russell, A. J. (1993). Obstacle marks produced by flow around stranded ice blocks during a glacier outburst flood (jökulhlaup) in west Greenland. *Sedimentology*, **40**, 1091–1111.

Saar, M. O. and Manga, M. (1999). Permeability-porosity relationship in vesicular basalts. *Geophysical Research Letters*, **26** (1), 111–114.

Saar, M. O. and Manga, M. (2004). Depth dependence of permeability in the Oregon Cascades inferred from hydrogeologic, thermal, seismic, and magmatic modeling constraints. *Journal of Geophysical Research*, **109**, B04204, doi:10.1029/2003JB002855.

Scott, E. D. and Wilson, L. (1999). Evidence for a sill emplacement on the upper flanks of the Ascraeus Mons shield volcano, Mars. *Journal of Geophysical Research*, **104** (E11), 27,079–27,089.

Sharp, R. P. and Malin, M. C. (1975). Channels on Mars. *Geological Society of America Bulletin*, **86**, 593–609.

Smith, D. E., Zuber, M. T., Frey, H. V. *et al.* (1998). Topography of the northern hemisphere of Mars from the Mars Orbiter Laser Altimeter. *Science*, **279** (5357), 1686–1692.

Stewart, S. T. and Nimmo, F. (2002). Surface runoff features on Mars: testing the carbon dioxide formation hypothesis. *Journal of Geophysical Research*, **107** (E9), 5069, doi:10.1029/2000JE001465.

Sugden, D. E., Clapperton, C. M. and Knight, P. G. (1985). A jökulhlaup near Søndre Strømfjord, west Greenland, and some effects on the ice-sheet margin. *Journal of Glaciology*, **31** (109), 366–368.

Tómasson, H. (1996). The jökulhlaup from Katla in 1918. *Annals of Glaciology*, **22**, 249–254.

Tschudin, K. (1946). Rate of evaporation of ice. *Helveticae Physica Acta*, **19**, 91–102.

Turcotte, D. L. and Schubert, G. (2002). *Geodynamics*, 2nd edn. Cambridge: Cambridge University Press.

Waitt, R. B. (2002). Great Holocene floods along Jökulsá á Fjöllum, north Iceland. *Special Publications of the International Association for Sedimentology*, **32**, 37–51.

Wang, C. Y., Manga, M. and Hanna, J. C. (2006). Can freezing cause floods on Mars? *Geophysical Research Letters*, **33** (20), L20202.

Williams, R. M., Phillips, R. J. and Malin, M. C. (2000). Flow rates and duration within Kasei Valles, Mars: implications for the formation of a Martian ocean. *Geophysical Research Letters*, **27**, 1073–1076.

Wilson, L. and Head, J. W. (2002). Tharsis-radial graben systems as the surface manifestation of plume-related dike intrusion complexes: models and implications, *Journal of Geophysical Research*, **107** (E8), 10.1029/2001JE001593.

Wilson, L. and Head, J. W. (2004). Evidence for a massive phreatomagmatic eruption in the initial stages

of formation of the Mangala Valles outflow channel, Mars. *Geophysical Research Letters*, **31** (15), L15701, doi:10.1029/2004GL020322.

Wilson, L., Ghatan, G. J., Head, J. W. and Mitchell, K. L. (2004). Mars outflow channels: a reappraisal of the estimation of water flow velocities from water depths, regional slopes, and channel floor properties. *Journal of Geophysical Research*, **109**, E09003, doi:10.1029/2004JE002281.

Woodworth-Lynas, C. and Guigné, J. Y. (2004). Extent of floating ice in an ancient Echus Chasma/Kasei Valles valley system, Mars. In *Lunar and Planetary Science Conference XXXV*, Abstract 1571. Houston, TX: Lunar and Planetary Institute.

Zhang, Y. X. and Kling, G. W. (2006). Dynamics of lake eruptions and possible ocean eruptions. *Annual Review of Earth and Planetary Sciences*, **34**, 293–324.